

强太赫兹波的产生及其在非线性和研究中的应用

王天武^{1,2,3,4,5*}, 张凯^{1,2}, 魏文寅^{1,2}, 李洪波^{1,2,3,4,5}, 周志鹏^{1,2}, 曹岭^{1,2}, 李鸿^{1,2}, 方广有^{1,2,3,4,5}, 吴一戎^{1,2,3,4,5}¹广东大湾区空天信息研究院, 广东 广州 510700;²广东省太赫兹量子电磁学重点实验室, 广东 广州 510700;³中国科学院电磁辐射与传感技术重点实验室, 北京 100190;⁴中国科学院空天信息创新研究院, 北京 100101;⁵中国科学院大学电子电气与通信工程学院, 北京 100049

摘要 强场太赫兹波具有高的峰值功率,相应地,其电磁场分量强度也很大。当强场太赫兹辐射物质表面时,会诱发一系列新奇的反常变化,受到人们的广泛关注。本文首先介绍了常见的一些强场太赫兹发射源,如光电导天线、光学整流晶体、超材料等,随后介绍了强场太赫兹技术在物态调控方面的一些典型应用,主要包括强场驱动热载流子运动、相干电子或声子调控、强场自旋电子学、太赫兹荧光发射、太赫兹克尔效应、生物医学等。

关键词 超快光学; 强场太赫兹源; 强场太赫兹调控; 太赫兹应用

中图分类号 O433.1

文献标志码 A

DOI: 10.3788/CJL230797

1 引言

光谱学是材料科学与工程中物质物性表征的重要手段,具有许多独特优势,如无接触测量、灵敏度高、方便快捷等。随着科技的日益进步,光谱学领域包含的分支结构愈加庞大,各种复杂功能的光谱分析技术应运而生。超快光谱学是近些年迅速发展起来的一个重要学科,其在传统稳态光谱学的基础上引入时间自由度,将光与物质相互作用的过程细分到皮秒甚至更短时间尺度,从而能够研究物质中热载流子、声子、激子等一些准激发粒子的时间分辨动力学过程。目前,超快光谱学中使用的波长已覆盖电磁波谱线中的绝大部分波段,其应用范围也已深入到凝聚态物理、材料科学、生物医疗、国防等领域。太赫兹光谱学是超快光谱学的一个重要分支,是 20 世纪 80 年代发展起来的一门新兴技术,具有重要的科研应用价值。通常所说的太赫兹 (THz) 波是指频率在 0.1~10 THz (波长为 3 mm~30 μm) 之间的电磁波,也被称为“亚毫米波”或“太赫兹辐射”。处于该波段的电磁波具有很多优异的特性,如光子能量小、穿透性高、与分子振动和转动能级匹配、无辐射危害等,太赫兹技术也因此成为 21 世纪的新兴科学技术,被评为“改变世界的十大技术”之一,受到了各国政府的高度重视。

随着太赫兹技术的不断进步,太赫兹波的发射效

率越来越高,相对应的电磁场强度也越来越大,其电场分量可以轻易达到 MV/cm 量级,而其相应的磁场分量也能达到特斯拉量级。这样的太赫兹波辐照到样品上时,其电磁场势必会对物质中的物态进行调控,从而发生一系列非线性响应,如碰撞电离、谷间散射、太赫兹克尔效应等。研究这些非线性效应可为深入理解相关的物理现象提供帮助,同时也可促进超快光电子器件的发展。

本文主要围绕强场太赫兹技术介绍了一些常见的强场太赫兹源,随后针对强场太赫兹辐射在物态调控中的一些应用进行了简单介绍。

2 强场太赫兹波的产生

目前,人们通常借助光电导天线来产生强场太赫兹波,常用的强场太赫兹辐射产生途径还有光学整流、光学差频、激发等离子体、太赫兹自由电子激光、同步辐射、量子级联效应等。

2.1 光电导天线

光电导天线是常见的太赫兹发射源和探测器。光电导天线由半导体衬底、金属电极和偏置电源组成。偏置电源在金属电极上施加高电压,这样电极之间就会形成偏置电场。当能量高于半导体带隙的飞秒脉冲激光泵浦到金属电极中间的半导体衬底上时,价带中的电子就会被激发到导带上形成电子空穴对(即光生

收稿日期: 2023-05-05; 修回日期: 2023-06-05; 录用日期: 2023-06-13; 网络首发日期: 2023-06-25

基金项目: 国家自然科学基金(61988102,12274424,11904056)、广东省重点研发计划(2019B090917007)、广东省科技计划项目(2019B090909011)、广州市基础与应用基础研究项目(202102020053)

通信作者: *wangtw@aircas.ac.cn

自由载流子)。载流子在偏置电场的作用下加速运动,形成瞬态电流,从而辐射太赫兹波。影响光电导天线发射效率的因素有衬底材质、载流子寿命、偏置电压、电极间隙等。通过合理调整参数,光电导天线也可以获得强的太赫兹脉冲^[1]。1996年,Budiarto等^[2]利用GaAs制作了一个光电导天线,电极间隙为3cm,偏置电压最高可达45kV。该天线的太赫兹波发射场强可达到数百kV/cm。实验结果表明,光电导天线输出的太赫兹脉冲宽度、强度与激光重复频率、脉宽有关,这可以用瞬态电流辐射效应来很好地解释。改变衬底材料,如将衬底材料更换成ZnSe、SiC、GaN等,可以大幅度提高发射的太赫兹强度^[3-6]。金刚石对可见光-太赫兹波段的大部分光具有高透性能,并且其击穿电场高达10MV/cm,光损伤阈值也很高,这些性质使得金刚石成为产生强太赫兹辐射的完美材料^[1,7]。但是,金刚石的带隙较大,为5.46eV,需要使用紫外光泵浦,并且紫外激光器造价昂贵,限制了金刚石的进一步应用。

2.2 光学整流

当脉冲激光通过具有二阶非线性效应的电光晶体时,脉冲激光中的各子频率光之间会产生非线性差频过程,从而在介质内部产生一个直流极化电场,这一过程被称为“光学整流效应”^[8]。早在1971年,Shen研究团队^[9-10]就已经从理论和实验上验证了光整流可以产

生远红外-太赫兹波段辐射。此后,该方法不断得到改进,得到的聚焦太赫兹场强纪录也在不断被刷新。光整流以高效率、方便快捷等优点成为目前实验室条件下常用的强场太赫兹波产生方式。常见的光整流晶体有铌酸锂/钽酸锂^[11-13]、有机晶体^[14-16]、石英^[17-18]等。这些晶体普遍具有非线性系数和损伤阈值高、THz吸收效率低等优势,这也是产生强场的必要条件。

铌酸锂晶体是常见的太赫兹非线性晶体,其z轴方向具有高达168pm/V的非线性系数^[19]。但是,由于激发光和太赫兹的折射率差异比较大,当激发光平行入射至晶体时,以切连科夫形式辐射产生的太赫兹光的相速度小于激发光的群速度,即相位不匹配,导致太赫兹光在晶体中相干相消,大大降低了太赫兹波的发射效率。2002年,Hebling等^[20]通过倾斜波前技术(如图1所示),改变激发光的相平面与入射方向的夹角(使其满足相位匹配),大大提升了太赫兹发射效率^[11-13],发射效率达到了约1%,聚焦场强为1MV/cm。2021年,吴晓君课题组^[21]利用波前倾斜技术和低温调控,在铌酸锂中实现了单周期1.4mJ的太赫兹脉冲,800nm光转换效率达到了0.7%,聚焦峰值电场强度和磁场强度分别约为6.3MV/cm和2.1T。近期,该课题组又将此纪录刷新到了13.9mJ,光转换效率达到了1.2%^[13]。

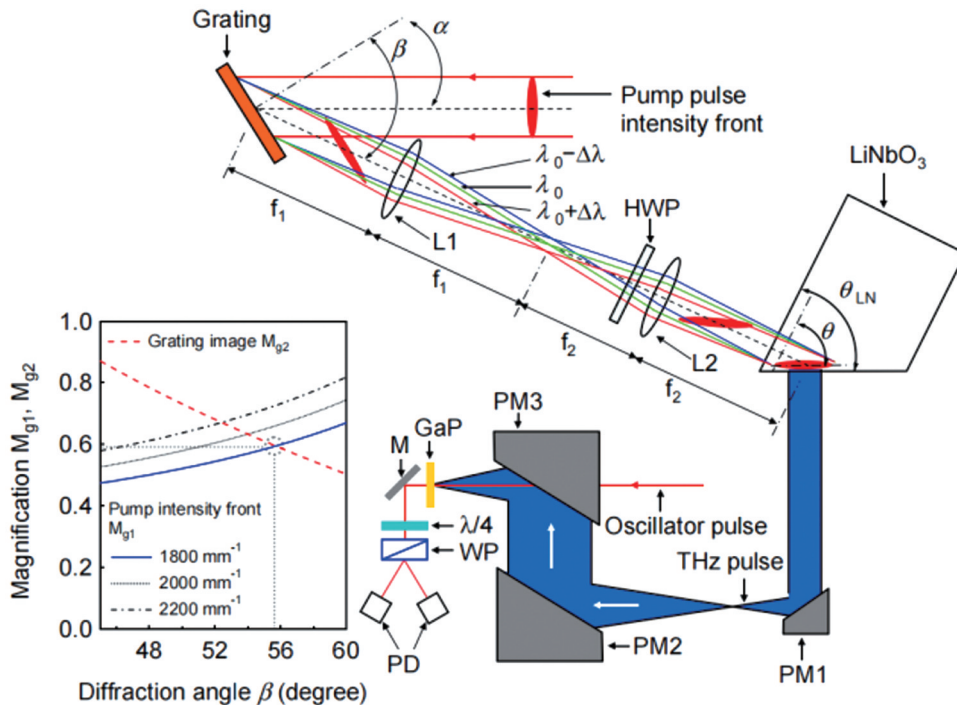


图1 LiNbO₃中的波前倾斜示意图^[20]

Fig. 1 Schematic diagram of the tilted-pulse front in LiNbO₃ crystal^[20]

有机晶体也是常见的强场太赫兹源。有机晶体一般具有非常高的非线性系数,可以发射高场强且宽带的太赫兹波。另外,大部分有机晶体的一个最大优势是近红外和太赫兹波段折射率的色散相对较弱,这使得太赫

兹波产生的相位匹配条件在有机物中几乎都可以得到满足,而不像LiNbO₃那样需要倾斜波前才能达到高的发射效率^[22]。早在1992年,Zhang等^[23]就发现有机晶体dimethyl amino 4-N-methylstilbazolium tosylate

(DAST)具有非常强的光学整流效应(比 GaAs 和 LiTaO_3 分别高 1 个和 2 个数量级),可以发射非常强的太赫兹波。这项工作引起了全球研究人员的关注,随后许多基于有机晶体的太赫兹源被陆续报道。目前,一系列有机晶体陆续被发现,如 DAST^[23-24]、DSTMS^[24-25]、OHI^[24,26]、PNPA^[27]等,都具有非常高的太赫兹发射强度。最近发现的 PNPA^[27]的太赫兹发射效率超过了非线性晶体 DAST 和 OHI,PNPA 在文献实验条件下产生了 2.9 MV/cm 的峰值场强,太赫兹发射效率超过了 4%。

2.3 激发等离子体

飞秒激光激发空气产生等离子体丝也是常见的强场太赫兹波产生方式。常见的系统是双色场系统。飞秒激光激发倍频晶体产生倍频光,剩余光通过另一个双折射晶体调整相位,使其与倍频光相位一致,双色脉冲同时激发空气成丝,产生强场宽带太赫兹波。2000

年,Cook 等^[28]首次在实验中观察了空气电离产生太赫兹辐射的现象,他们利用 65 fs、800 nm、150 μJ 光产生了约 2 kV/cm 的太赫兹脉冲。2014 年,Oh 等^[29]利用 30 fs、15 mJ 脉冲光激发空气,产生了高达 8 MV/cm 的太赫兹脉冲,其频谱宽度覆盖 0.1~10 THz。2020 年,Koulouklidis 等^[30]使用 TW 级 3.9 μm 中红外飞秒激光产生了强度高达 100 MV/cm 的太赫兹波,能量转换效率达到了 2.36%。笔者课题组搭建了空气等离子体成丝发射系统,系统示意图如图 2 所示。通过该系统获得了带宽为 1~35 THz 的太赫兹光谱,太赫兹波的聚焦峰值强度达到了 100 kV/cm,光谱如图 3 所示。此外,笔者课题组还利用该系统研究了 Mxene 薄膜的吸收特性^[31]。目前,激发空气等离子体辐射太赫兹波的物理解释有很多,例如四波混频模型、光电流模型、瞬时切连科夫辐射模型等。

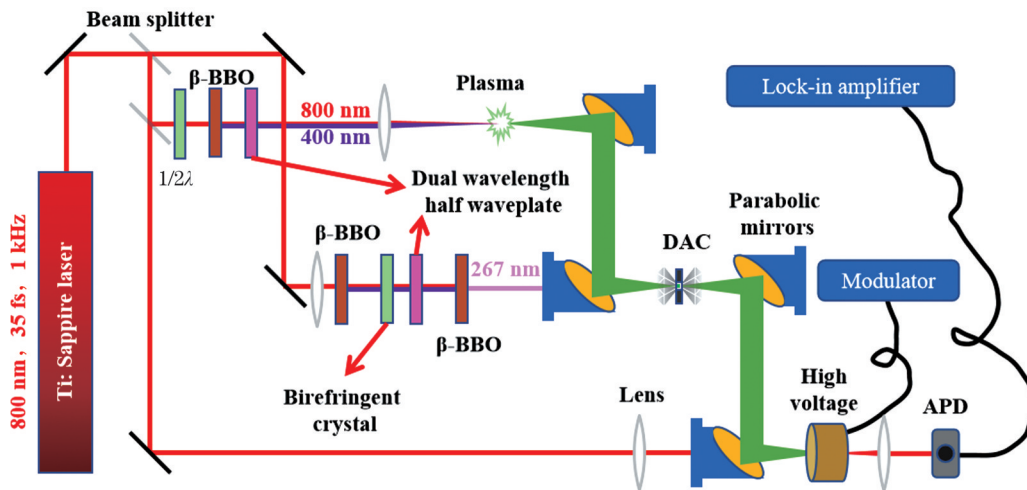


图 2 空气等离子体成丝发射太赫兹装置示意图(DAC 为金刚石对顶砧,它能够产生静水压环境)

Fig. 2 Schematic diagram of air plasma terahertz source device (DAC: diamond anvil cell, a setup can generate hydrostatic pressure condition)

除空气外,飞秒激光激发固体或液体介质也可以产生强太赫兹脉冲^[32-34]。1993 年,Hamster 等^[35]利用飞秒激光辐照镀铝玻璃片靶材,在透射方向上观测到了远红外-太赫兹波段的电磁波辐射。2005 年,盛政明等^[36]发现,当脉冲激光斜入射到非均匀密度梯度的等离子体上时,激光尾迹场通过线性模式转换可以在等离子体振荡频率附近产生强相干太赫兹发射。2015 年,Liao 等^[37]利用脉宽为 0.5 ps 的脉冲光轰击铜基靶材,在反射方向上观测到了最高达 0.23 mJ/sr 的太赫兹发射。2019 年,上海交通大学的 Liao 等^[38]利用高强度皮秒脉冲激光轰击金属箔,产生了能量最高可达 50 mJ 的太赫兹脉冲,该值比其他十分先进的太赫兹源产生的太赫兹脉冲能量高出近一个数量级。虽然光与固体或液体介质作用能产生超强的宽谱太赫兹脉冲,但也存在一些缺点,如转换效率低(通常小于 0.1%),受靶材密度、压力、处理方式等以及入射激光角度、偏振等因素的影响较大,影响其实验室适用性。

2.4 超材料表面增强太赫兹

通过人工设计图案,将子单元按照一定的结构周期性排列,可以勾勒出一系列复合超材料,这些复合超材料可以表现出与所构成材料不同的超常物理性质。1998 年,Ebbesen 等^[39]设计了基于金属薄膜的亚微米圆柱腔阵列,当波长大于阵列周期的入射光照射到阵列表面时,透射强度比孔径理论预测的强度高几个数量级,即出现明显的透射增强。这一发现迅速被广泛利用,尤其是在太赫兹技术领域,因为太赫兹波的波长很长,金属微结构的尺寸相对较大,易于加工。2009 年,Seo 等^[40]在金属薄膜上设计了不同尺寸的狭缝,该结构相当于一个纳米尺寸的电容器,当辐照交流电场(太赫兹波)时,该结构会对电场进行放大,如图 4 所示。当狭缝宽度为 70 nm 时,0.1 THz 处的电场强度被放大了约 800 倍。开口谐振环(SRR)是目前常见的太赫兹超材料。2012 年,Liu 等^[41]设计一个 SRR,并研究了 VO_2 材料的绝缘体-金属相变,如图 5 所示。模拟

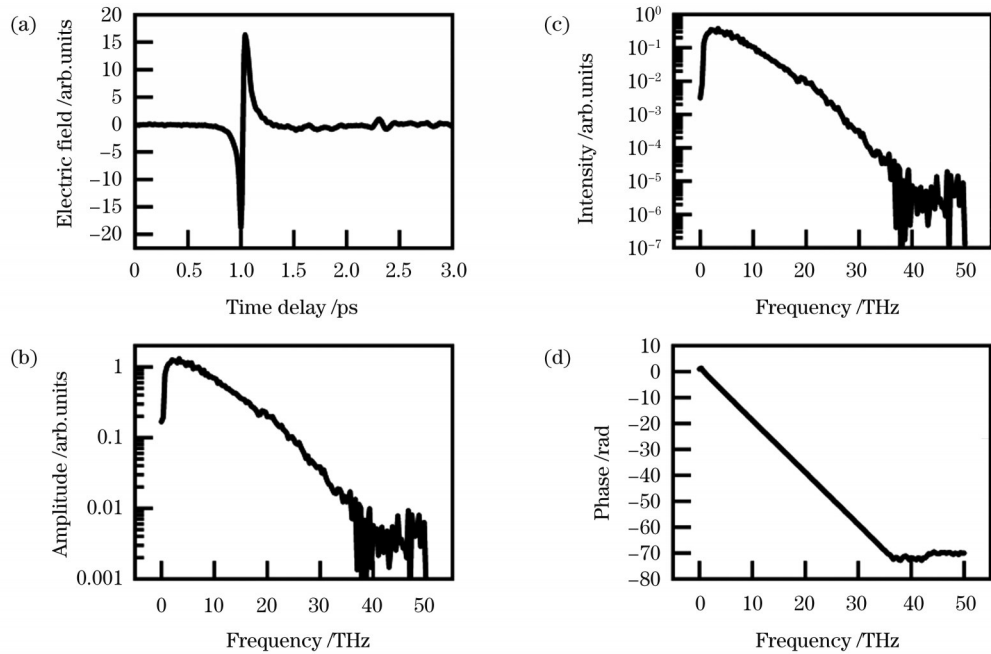


图3 实验室宽带太赫兹光谱。(a)时域光谱图;(b)快速傅里叶变换后的频谱幅度图;(c)频谱幅度的平方;(d)快速傅里叶变换后的相位图

Fig. 3 Ultrabroad terahertz spectra obtained in our laboratory. (a) Time-domain spectrum; (b) frequency-domain spectrum after fast Fourier transform (FFT); (c) square of the frequency-domain amplitude; (d) phase spectrum after FFT

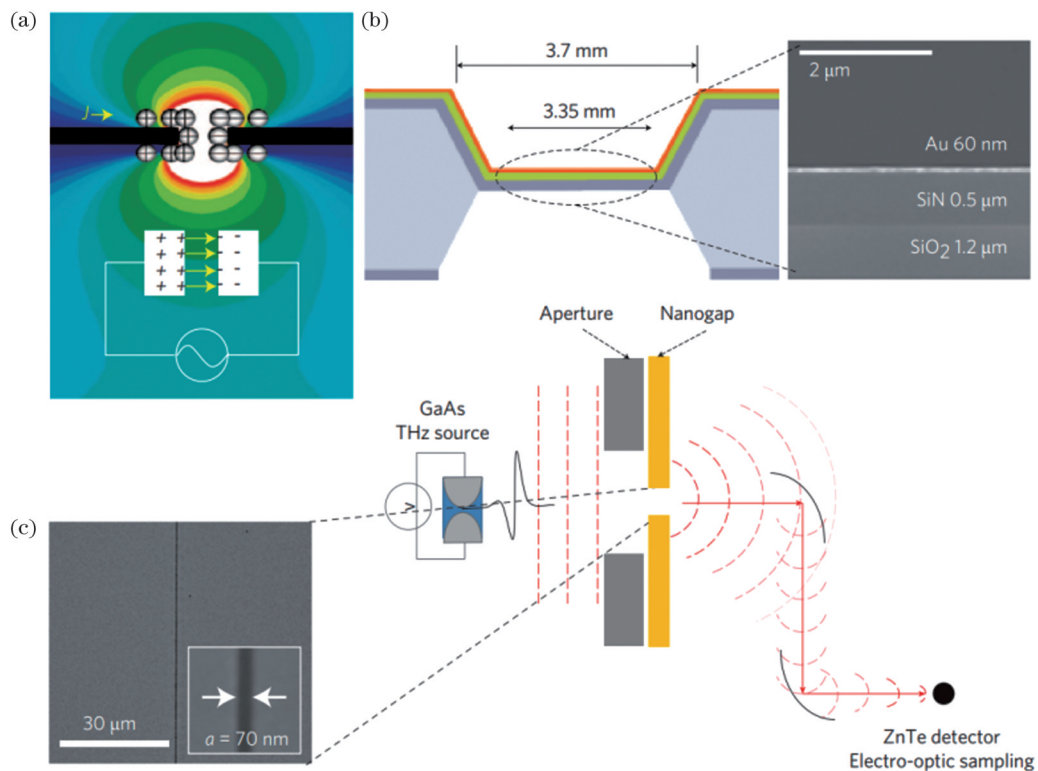


图4 太赫兹超表面纳米间隙和时域光谱学^[40]。(a)光感应交流电对纳米间隙进行充电,增强电场,如渐变的彩色轮廓所示;(b)聚焦离子束加工前近乎独立的纳米间隙样品结构截面以及主面板区域的扫描电子显微镜(SEM)图像;(c)电光采样测量样品的太赫兹时域光谱,其中展示了纳米间隙的几何形状和尺寸(金膜上加工了一个70 nm宽的间隙)

Fig. 4 Terahertz metasurface nanogap and time-domain spectroscopy^[40]. (a) Light-induced alternating current charges the nanogap, thereby enhancing the electric field as represented by the gradual colour contour; (b) a cross-section of the nearly free-standing nanogap sample structure before FIB (focus ion beam) processing and a scanning electron microscopy (SEM) image of the area indicated in the main panel; (c) terahertz time-domain spectroscopy of the sample is measured by electro-optic sampling, where an SEM image shows the geometry and dimensions of the nanogap (a 70 nm width nanogap perforated on gold film)

结果显示,约 300 kV/cm 的太赫兹波入射到裂纹处,峰值场强可增大到 4 MV/cm,该强度已远大于 VO₂ 的相变阈值,甚至会使 VO₂ 薄膜出现不可逆损伤。

超材料增强太赫兹也有一定的局限性,因为一旦超材料子单元的结构、空间排列方式、材质等确定后,

其谐振频率和强度、极化方向和相位等参数也会随之确定,具有一定的使用局限性。将可调节材料,如形变材料、液晶材料、二维材料等,作为支撑材料设计超材料,可以利用电学、热学、光学等外部激励来改变超材料的性质,从而实现太赫兹波的动态调控^[42-43]。

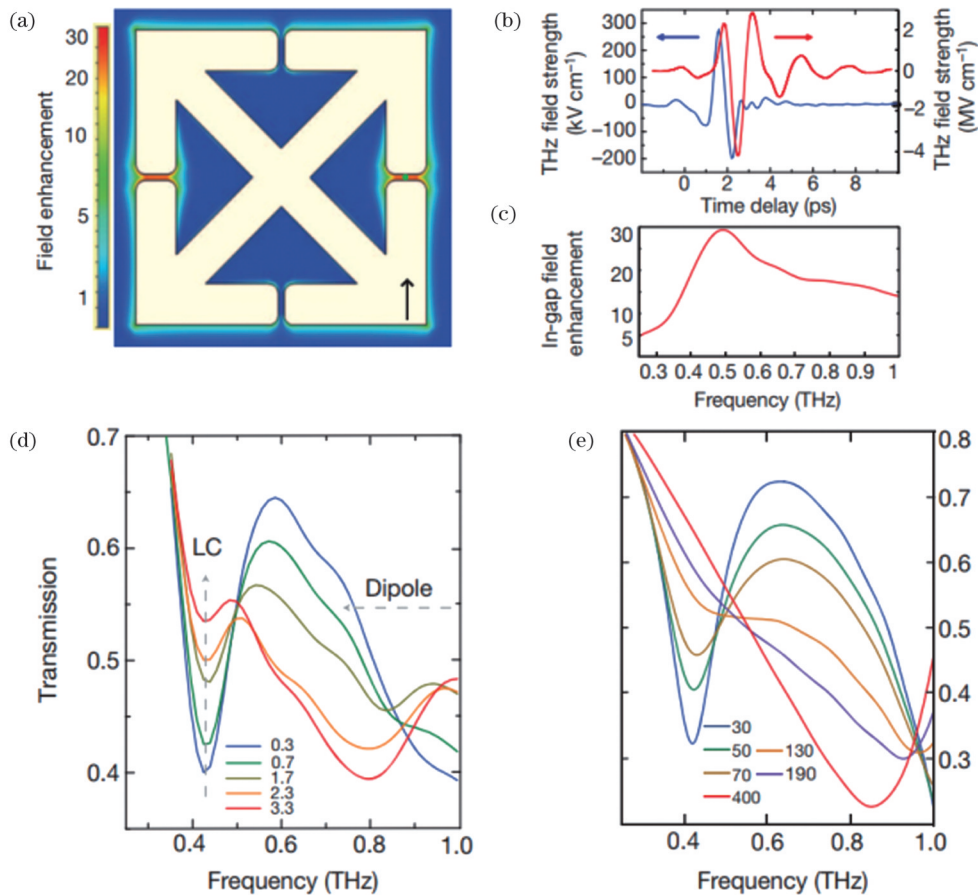


图 5 SRR 和非线性太赫兹透射实验中电场增强的全波模拟^[41]。(a)共振场增强作为位置的函数;(b)以实验数据(蓝色)作为输入,模拟水平间隙中随时间变化的太赫兹场强(红色);(c)由模拟的间隙内场强和测量的入射场强之间的傅里叶幅值之比得到的隙内场增强的频率依赖关系;(d)在 324 K、0.3~3.3 MV/cm 的间隙场强范围内,分布在 VO₂ 上的 SRRs 的非线性透射光谱;(e)隙内电导率在 30~400(Ω·cm)⁻¹ 范围内时 SRR 响应的全波模拟(假设实部电导率 σ_1 仅在隙内变化)

Fig. 5 Full-wave simulations of the electric field enhancement in the SRR and nonlinear THz transmission experiment^[41]. (a) Resonant field enhancement as a function of position; (b) simulated time-dependent THz field strength (red) in the horizontal gaps using experimental data (blue) as the input; (c) frequency-dependent in-gap field enhancement obtained from the ratio of Fourier amplitudes of the simulated in-gap and measured incident fields in Fig. (b); (d) field-dependent nonlinear transmission spectra of SRR on VO₂ at 324 K, for in-gap field strength ranging from 0.3 to 3.3 MV/cm; (e) full-wave simulations of SRR response for in-gap conductivities ranging from 30 to 400 (Ω·cm)⁻¹ (assuming real part conductivity σ_1 changes only in the gaps)

2.5 针尖增强太赫兹

针尖的天线效应是一种增强电场的有效方式^[44-45]。当激光照射到针尖尖端时,纳米尺度的尖端结构会在尖端附近表面诱导一种高度局域化的特殊的电场传播模式,也就是等离激元^[45]。这种特殊的表面电场能以指数倍增加入射光的太赫兹波电场强度^[46]。特别地,当针尖与样品的距离为 1 nm 时,可实现约 10⁵ 倍电场增强^[47]。同时,由于针尖的局域效果,光耦合后可以具备超越衍射极限的空间分辨能力。2017 年,Hegmann 课题组^[47]首次将太

赫兹脉冲耦合到扫描隧道显微镜 (STM) 的扫描探针尖端来调制 STM 偏压,并证明了太赫兹脉冲能够诱导 STM 隧穿电流。THz-STM 在实验室环境条件下能同时提供亚皮秒 (<500 fs) 的时间分辨率和纳米量级 (2 nm) 的成像分辨率,可以直接实现到单个 InAs 纳米点的超快成像。随后,该技术快速发展,突破了传统分辨率^[48-49],如图 6 所示。笔者所在研究团队以铌酸锂为太赫兹源,搭建了一套高时空分辨的太赫兹扫描隧道显微镜 (THz-STM),研究了太赫兹脉冲对隧穿电流的作用过程,进而实现了对单分子

或原子电子轨道波函数的超快成像,装置如图 7(a) 所示。本团队利用太赫兹自相关系统对 STM 系统进行了表征,结果如图 7(b) 所示。可以看到,太赫兹强度越弱,脉冲宽度越窄,时间分辨率越高,本团

队搭建的系统能达到最低 350 fs 的时间分辨率。本团队又利用太赫兹波(作为偏置电压)产生隧穿电流,对硅(111)面进行了成像,如图 7(c) 所示,空间分辨率能达到 0.1 nm。

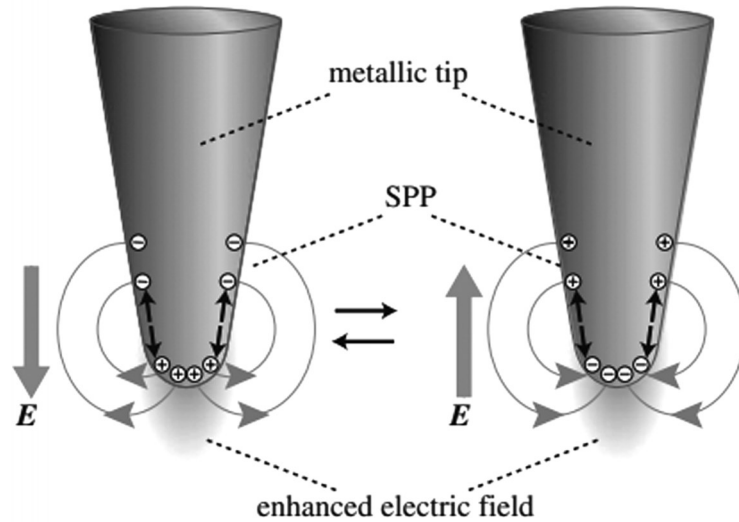


图 6 针尖等离子激元增强电场^[45]

Fig. 6 Localized surface plasmon polariton enhancing field at the metallic tip apex^[45]

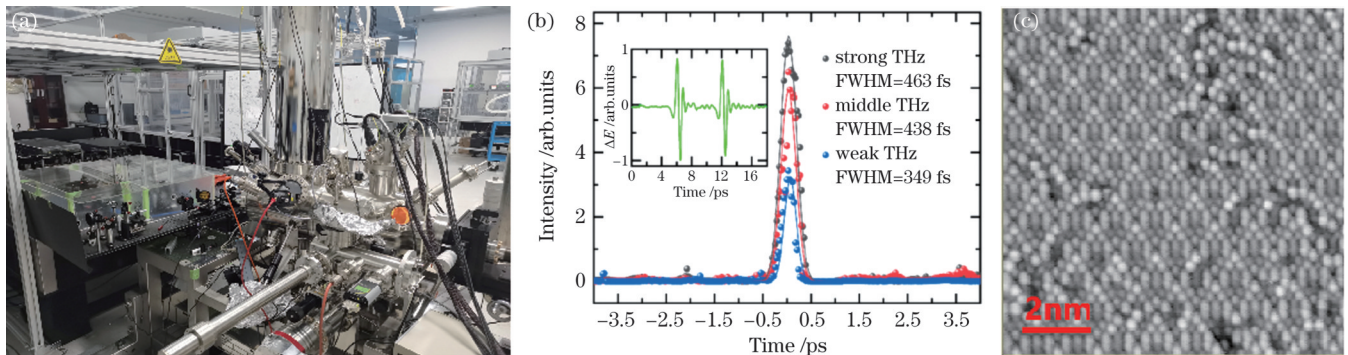


图 7 THz-STM 实物图及其应用。(a) 广东大湾区空天信息研究院大湾区分院搭建的 THz-STM; (b)~(c) 仪器测量的自相关信号和硅表面图像(时间分辨率约为 350 fs, 空间分辨率约为 0.1 nm)

Fig. 7 THz-STM and its applications. (a) THz-STM in GBA Branch of Aerospace Information Research Institute, Chinese Academy of Sciences; (b)–(c) measured autocorrelation signal and silicon surface image (the temporal resolution is about 350 fs and the spatial resolution is about 0.1 nm)

3 强场太赫兹波的应用

3.1 强场驱动热载流子运动

当太赫兹电场辐射半导体材料时,样品中的载流子在电场作用下获得动量,沿电场方向移动。当太赫兹电场强度较弱时,载流子在移动过程中主要受到杂质、缺陷、声子等的作用发生散射,并不会直接与原子发生作用。当电场强度增大时,载流子动能变大,此时载流子就有一定的概率与原子发生作用并电离它们。碰撞过程中会额外产生一对电子和空穴,新的载流子在电场的加速下会电离出更多的载流子,从而使电导率明显增大,太赫兹透射率急剧减小。Markelz 等^[50]在用远红外-太赫兹波段的光辐照 InAs/Al_{1-x}Ga_xSb 异质结时发现,其透射率在场

强超过 3 kV/cm 时突然下降了约 50%。通过直流电导的测量和分析发现,透射率下降源于碰撞电离引起的载流子密度的迅速增加。2017 年, Tarekegne 等^[51]利用 MV/cm 量级的太赫兹波激发硅样品,结合超快光泵浦-探测技术研究了硅的碰撞电动力学。他们在实验中发现了明显的由载流子倍增效应导致的反射增强现象,如图 8 所示,并发现倍增因子随着初始载流子密度的增大而减小。

另外,在一些多能谷半导体材料中,载流子在强太赫兹辐射作用下动量增加。当材料中最低能谷附近存在能量接近的能谷时,移动的载流子就会迁移到该能谷,发生谷间散射^[52-53]。一般情况下,这两个能谷的色散特性不一样,这就导致跃迁后的载流子有效质量发生变化,进而导致迁移率等性质发生变

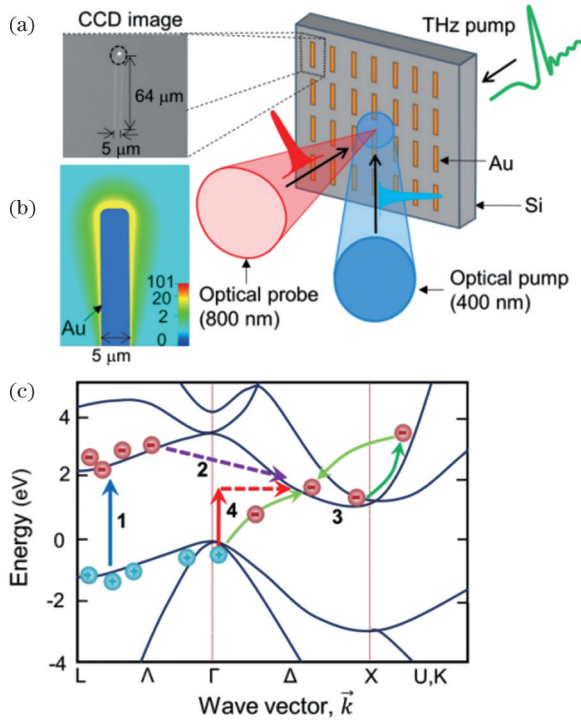


图 8 硅中太赫兹诱导碰撞电离的探测^[51]。(a)用于研究硅中太赫兹诱导碰撞电离(IMI)的泵浦探测装置示意图,图中显示了带有明亮探测点(虚线圆)的天线阵列单元格的 CCD 图像;(b)计算得到的天线尖端附近局部电场增强分布图;(c)硅能带结构中的载流子跃迁:由泵浦光引起的带间跃迁(1),L 到 X 谷的谷间散射(2),IMI 引起的载流子倍增(3),声子辅助的带间跃迁(4)

Fig. 8 Investigation of the THz-induced impact ionization in silicon^[51]. (a) Schematic diagram of the pump-probe setup used to investigate THz-induced IMI in silicon, where a CCD image of unit cell of the antenna array with bright probe spot (dashed circle) is shown in the inset; (b) calculated local electric field enhancement profile near the antenna tip; (c) carrier transitions in silicon band structure: interband transitions due to pump beam (1), L-to-X intervalley scattering (2), carrier multiplication through IMI (3), and phonon-assisted interband transition (4)

化,最终影响太赫兹光谱特性。2009年,Su等^[52]利用光泵浦-铈酸锂源强场太赫兹探测技术研究了 GaAs 中的超快载流子弛豫动力学。他们在实验中使用 800 nm 光泵浦 GaAs,结果发现使用强场探测的透射率变化比使用弱场探测的透射率变化明显降低。这是因为:GaAs 是多能谷半导体,泵浦光激发的热载流子布居在 Γ 谷,如图 9 所示,在弱场探测下,载流子逐步回落到谷底,与空穴复合,而在强场探测下,载流子发生谷间散射,跃迁到邻近的 L 谷。由于 L 谷比较平坦,电子的有效质量大、迁移率低,从而有效降低了电导率,使泵浦调制信号变低。相关的谷间散射参数还可以使用谷间电子跃迁模型拟合得到^[54]。

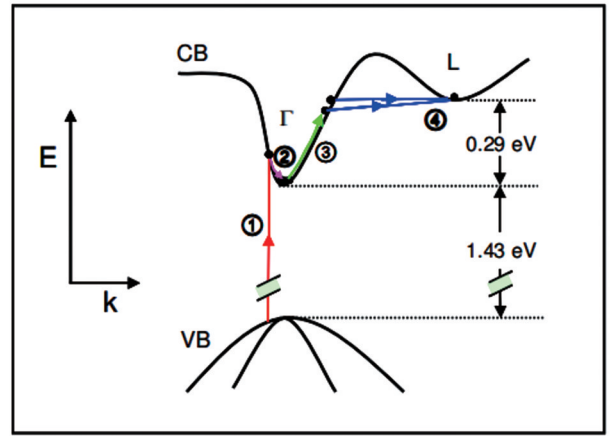


图 9 GaAs 的电子能带结构示意图及相关激发机制^[52]。① 800 nm 泵浦光激发 GaAs 样品中的电子和空穴,电子被注入到导带中迁移率较高的中心 Γ 谷中。② 电子在 1 ps 内迅速热化到 Γ 谷底部。③~④ 强场太赫兹探测脉冲将 Γ 谷中的光激发电子加速到更高的能量,这可能会导致向 L 谷的谷间散射

Fig. 9 Schematic of the electronic band structure of GaAs and related excitation mechanisms^[52]. ① The 800 nm pump pulse excites electrons and holes in the normally insulating GaAs sample, with the electrons being injected into the higher mobility central Γ valley in the conduction band. ② The electrons quickly thermalize within 1 ps to the bottom of the Γ -valley. ③-④ A high-field THz probe pulse accelerates the photoexcited electrons to higher energies in the Γ -valley, which may result in intervalley scattering to the L-valley

3.2 强场驱动电子和晶格位移——相干调控

当脉冲光与物质相互作用时,常常会引发物质内一些声子模式的同相位振动,即产生相干声子振动,此时介电函数会发生周期性调制。当调制发生到一定程度时,还会诱导瞬态甚至不可逆的电子或晶格结构转变,引发一系列新奇的物理现象。传统上,短脉冲激光激发可以诱导相干声子,该过程是通过热载流子激发以及热载流子在弛豫过程中与声子的交换来实现的^[55-57]。但是,热电子的激发也会反过来影响相干声子的一些参数并可能导致样品损坏。强太赫兹激发也可以有效激发相干声子。一些红外模式的能量正好处于太赫兹波段,太赫兹波入射时能与其共振激发产生相干声子。不仅如此,当太赫兹强度达到一定程度后,还可以发生合频^[58]和非线性耦合^[59-60],诱导出拉曼激活模式。另外,脉冲强太赫兹波的电场分量也可以瞬间驱使电荷极化,原子位置发生移动,脉冲撤去后原子发生相干振荡^[61-63]。强场太赫兹波的这种相干晶格扰动在铁电材料中的应用比较广泛。电场可以诱导出电偶极矩,从而控制亚纳秒时间尺度上的超快铁电极化,因此在高速非易失性存储器、电光调制器、压电调制器等光电器件领域具有一定的应用潜力^[64-66]。2019年,Sie等^[61]里利用强场太赫兹激

发 Weyl 半金属 WTe_2 , 并用超快电子衍射来获取不同时间时的晶格结构, 装置示意图和结果如图 10 所示。结果表明, 当太赫兹电场激发半金属 WTe_2 后, 会诱导 WTe_2 的层间剪切应变, 产生相干声子振荡, 而且这种光学方法产生的内部应力要比传统压电方法产生的大一个量级以上。实验中还发现, 相干振荡的幅

度和频率随着太赫兹电场的增大而改变, 并且在 7.5 MV/cm 的场强下, 晶格移位达到了 8 pm , 并且进入了一个新的平衡态, 该平衡态可以持续 70 ps 以上。模拟计算还表明, 这种晶格移位还可以调制半金属 WTe_2 本身的 Weyl 点性质。相同的现象在 ZrTe_5 中也有体现^[62]。

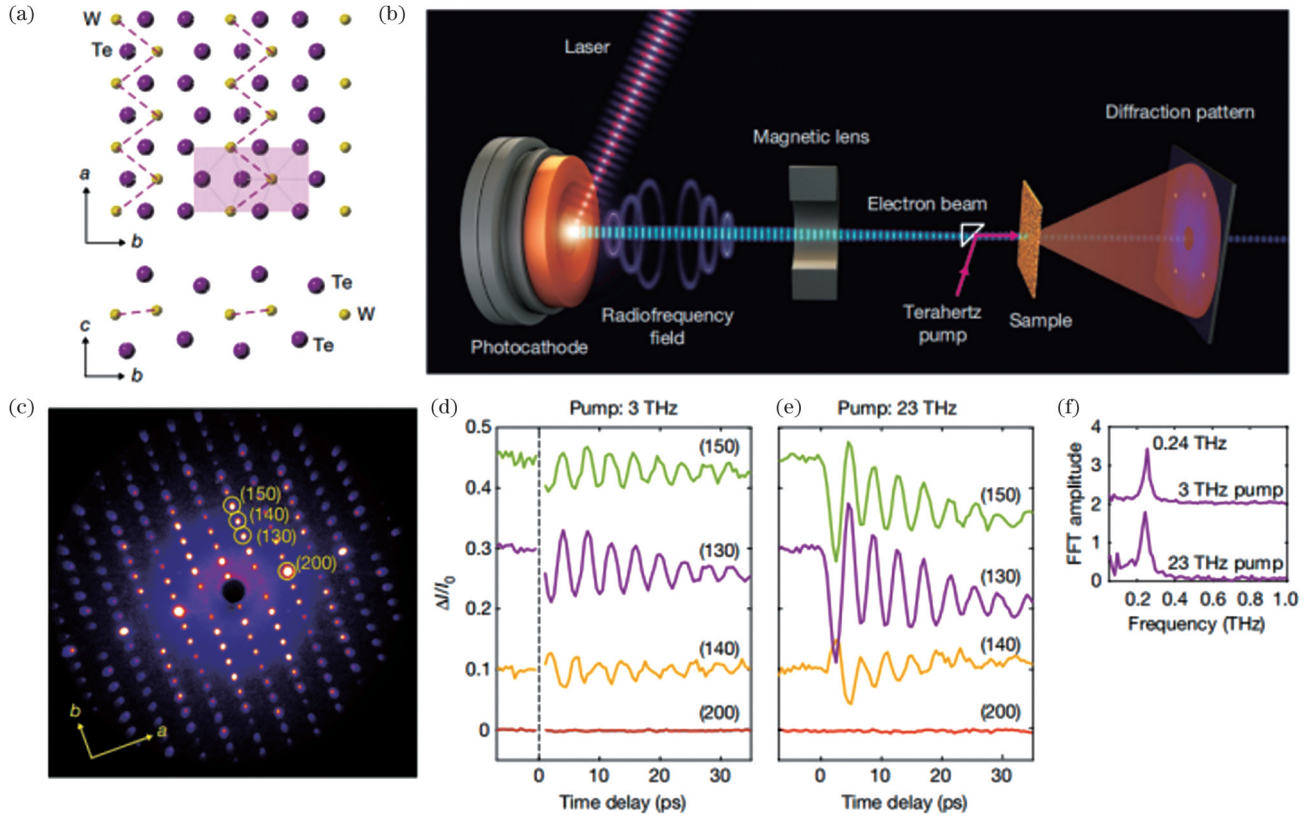


图 10 用相对论超快电子衍射法测量 WTe_2 中的相干层间剪切模式^[61]。(a) Td-WTe_2 的晶格结构; (b) SLAC 3-MeV 相对论超快电子衍射装置示意图 (利用强太赫兹脉冲泵浦诱导 WTe_2 的层间剪切应变); (c) 平衡态 WTe_2 的电子衍射图谱; (d)~(e) 布拉格峰强度随太赫兹泵浦脉冲与电子束之间时间延迟的变化; (f) 相干振荡的快速傅里叶变换振幅, 其表示的是沿 b 轴的 0.24 THz 剪切声子模式

Fig. 10 Coherent interlayer shear mode in WTe_2 measured using relativistic ultrafast electron diffraction^[61]. (a) Lattice structure of Td-WTe_2 ; (b) schematic of SLAC 3-MeV relativistic ultrafast electron diffraction setup (intense terahertz pump pulses are used to induce interlayer shear strain in WTe_2); (c) measured electron diffraction pattern of WTe_2 at equilibrium. (d)~(e) changes in Bragg peak intensity as a function of time delay between the terahertz pump pulses and the electron beam; (f) FFT amplitude of the coherent oscillation, indicating the 0.24 THz shear phonon mode along the b axis

3.3 强场自旋电子学

磁性材料作为一种重要的功能材料, 与太赫兹之间的交叉研究受到了越来越多的关注。当太赫兹辐射到磁性材料上时, 太赫兹磁场分量会以 Zeeman 力矩的形式作用于磁性材料的磁矩, 从而使其离开平衡位置, 产生磁进动^[67]。因交换作用耦合在一起的磁矩协同进动在宏观上可形成自旋波。自旋波具有能量耗散极低的优点, 利用自旋波可以制备出功耗极低的功能性器件, 因此, 利用太赫兹相干调控自旋波具有重要的应用价值^[68]。对于反铁磁有序的磁性材料, 因磁矩之间的强交换作用, 其磁矩进动频率能够达到 THz 量级, 因此, 其在太赫兹辐射的磁场分量作用下通常表现出共

振自旋波激发; 而对于铁磁有序的磁性材料, 其进动频率在 GHz 量级, 表现为非共振激发^[69-71]。

2011 年, Kampfrath 等^[67] 利用连续两束峰值磁场强度为 0.13 T 的太赫兹波, 通过控制两束脉冲之间的时间间隔, 实现了 NiO 中本征频率为 1.0 THz 的自旋波的相干性调控, 如图 11 所示。2013 年, Jin 等^[72] 利用同样的原理, 借助磁光晶体 YFeO_3 的双折射特性, 实现了单脉冲太赫兹波对 YFeO_3 中自旋波的相干调控。此外, 利用太赫兹辐射还可以驱动反铁磁材料中的自旋与晶格之间的耦合。2021 年, Mashkovich 等^[73] 利用太赫兹辐射激发反铁磁材料 CoF_2 , 通过体系中磁振子与声子之间的耦合, 实现了太赫兹声子的激发, 如图 12 所示。

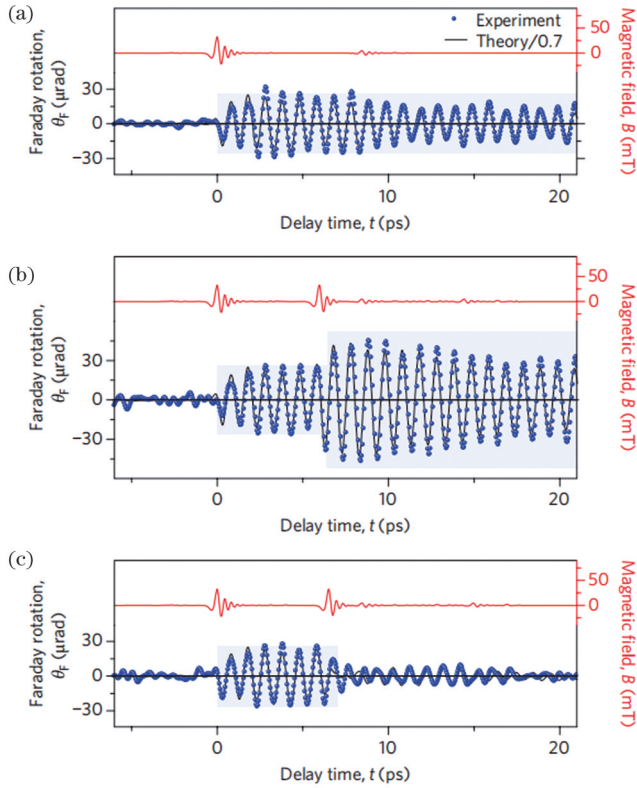


图 11 自旋波的相干太赫兹调控^[67]。(a)由单个太赫兹脉冲磁场分量(红色曲线)引起的法拉第旋转(点:实验结果;线:数值模拟结果);(b)两个脉冲(红色曲线)相互延时 $\Delta t=6$ ps 时激发相干磁振子振荡,随后,其振幅提高了近 2 倍(阴影区域);(c) $\Delta t=6.5$ ps 时相干激励磁振子的产生和消失

Fig. 11 Coherent terahertz control of spin waves^[67]. (a) Faraday rotation (dots: experimental results; line: numerical simulation) induced by a single terahertz magnetic pulse (red curve); (b) excitation by two pulses (red curve) with a mutual time delay of $\Delta t=6$ ps launches a coherent magnon oscillation and, subsequently, enhances its amplitude by a factor of almost 2 (shaded area); (c) excitation with $\Delta t=6.5$ ps switches the magnon on and off coherently

随着太赫兹波磁场强度的增加,受激发的磁矩动力学学会表现出非线性特征。2016年,Baierl等^[74]利用峰值磁场强度为 0.4 T 的太赫兹波激发 NiO 后发现激发出的自旋波包含 1.0 THz 的二次谐波分量。

利用太赫兹波也可以实现对磁性材料磁矩的超快调控,这种超快调控磁矩的方法对于实现超快写入的磁存储器件具有重要意义。2013年,Vicario等^[75]利用峰值磁场强度为 0.4 T 的单周期太赫兹脉冲激发 10 nm 厚 Co 薄膜,实现了对 Co 层磁矩皮秒量级的调控。

另外,在强场太赫兹脉冲与磁性材料尤其是厚度在纳米量级的铁磁性金属薄膜相互作用过程中,太赫兹波电场分量对磁性调控也有着很大影响。2016年,Bonetti等^[76]利用峰值电场强度为 60 MV/m 的单脉冲太赫兹波分别激发单晶 Fe 薄膜与多晶 CoFeB

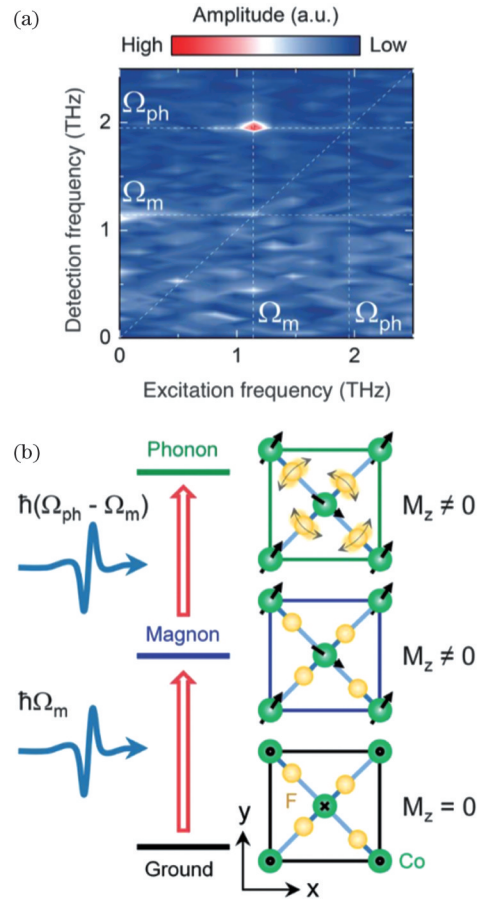


图 12 太赫兹光驱动晶格与自旋的耦合^[73]。(a)非线性振幅的二维傅里叶谱;(b)太赫兹磁场分量激发 B_{1g} 声子磁振子示意图。底部显示的是 CoF_2 单胞的无扰动反铁磁态。太赫兹光子以 Ω_m 频率共振填充相干磁态,从而产生中间态。另一个频率为 $\Omega_{ph}-\Omega_m$ 的太赫兹光子与这个中间态相互作用相干激发 B_{1g} 声子

Fig. 12 THz light-driven coupling of lattice to spins^[73]. (a) Two-dimensional Fourier spectrum of the nonlinear amplitude; (b) a pictorial of the magnon-mediated excitation of the B_{1g} phonon by a THz magnetic field. The unperturbed antiferromagnetic state of the CoF_2 unit cell is shown at the bottom. A THz photon resonantly populates the coherent magnonic state at the frequency Ω_m , thus creating an intermediate state. Another THz photon at the frequency of $\Omega_{ph}-\Omega_m$ interacts with this intermediate state and coherently excites the B_{1g} phonon

薄膜,结果显示:后者在太赫兹脉冲离开后会出现一定程度的退磁现象,而前者则未出现这种现象。他们将这种现象归结于太赫兹电场分量加速多晶 CoFeB 材料中的电子产生的超快自旋流由于晶格缺陷或杂质而被耗散掉,从而使样品在宏观上表现为磁性消失。对于单晶 Fe 薄膜,其缺陷数量较少,退磁现象并不显著。因此,在研究太赫兹脉冲对磁性金属薄膜超快调控的同时,有必要考虑电场分量带来的影响。

太赫兹波电场分量还可以用来对材料的磁矩进行间接调控^[76-77]。2016年, Baierl等^[78]利用太赫兹波电场分量共振激发 TmFeO₃材料中的 Tm³⁺, 使其发生能级跃迁(约为 1~10 meV), 如图 13 所示。因为 Tm³⁺参与

Fe³⁺之间的交换作用, 因此对 Tm³⁺的激发可以实现对材料磁各向异性的调控。这种瞬时磁各向异性的调控等效于给 Fe³⁺磁矩施加了一个力矩, 从而改变了太赫兹波幅值, 实现了非热超快磁矩翻转。

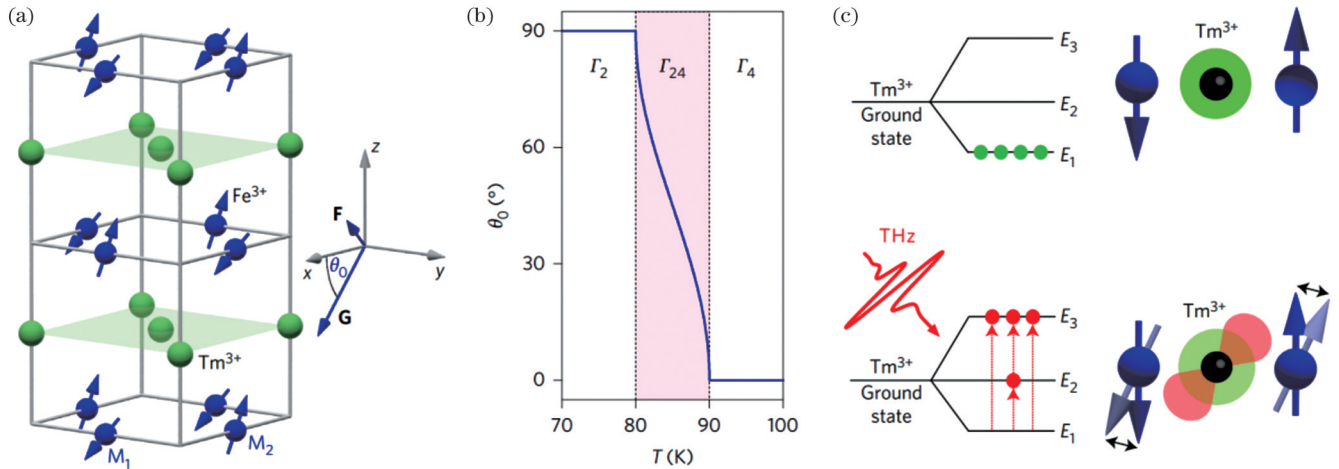


图 13 太赫兹辐射诱导的各向异性力矩控制自旋的原理^[78]。(a) Γ_{24} 相中 TmFeO₃的自旋和晶格结构;(b) 自旋重取向相变;(c) 晶体场将稀土 Tm³⁺离子的基态 3H6 分裂成能量间隔约为 1~10 meV 的几个能级(上图:相应的轨道波函数确定了铁离子自旋在热平衡状态下的磁各向异性;下图:由太赫兹脉冲共振诱导的能级之间的超快跃迁对自旋施加突变扭矩,并作为相干自旋动力学的有效触发器)

Fig. 13 Principle of spin control by a terahertz-induced anisotropy torque^[78]. (a) Spin and lattice structure of TmFeO₃ in the Γ_{24} phase; (b) spin reorientation phase transitions; (c) the crystal field splits the ground state 3H6 of the rare-earth Tm³⁺ ions into several energy levels with an energy spacing of $\sim 1-10$ meV (upper panel: the corresponding orbital wavefunctions set the magnetic anisotropy for the iron spins in thermal equilibrium; lower panel: ultrafast transitions between these energy levels resonantly induced by terahertz pulses should exert an abrupt torque on the spins and act as an efficient trigger for coherent spin dynamics)

除了上述研究课题以外,太赫兹技术与磁性材料的交叉研究还包含其他具有重要应用价值的课题,例如基于自旋的太赫兹辐射源等^[79]。随着研究的不断深入,二者的交叉研究必定能够取得更多有意义的成果。

3.4 太赫兹波上转换荧光

当入射半导体材料的太赫兹场达到一定阈值时可发生碰撞电离,继续增加太赫兹波强度甚至可以发生场电离,即太赫兹场直接把原子外的电子剥离出去,从而直接激发半导体材料产生荧光^[80-82]。2017年, Nelson课题组^[82]利用一块基于金属微间隙阵列的场增强结构将太赫兹场强增大到了 2~15 MV/cm,并在间隙中观察到了明显的太赫兹波驱动的 CdSe-CdS 核-壳量子点发光现象。实验证明,强场太赫兹波可以产生强的 Stark 效应,诱使量子点能隙高且快的调制,从而诱导发光。2019年, Liao等^[80]在硅中也观察到了太赫兹辐射诱导的荧光产生。尽管硅的带隙(1.12 eV)超过了中心太赫兹光子能量的 1000 倍,如果太赫兹波场足够强,仍将出现带间发光。使用科研级相机可以在太赫兹焦斑内观察到明亮的近红外发光,发光强度随着太赫兹能量增加呈指数增长;当场强为 0.08 GV/m 时,光斑直径为 3 mm 的太赫兹入射到硅样品上的能量为 100 μ J 时便达到饱和。另外,由于碰撞电离的非线性行为,实验中观察到的发光强度随太赫兹能量增大呈非线性增加。

太赫兹驱动非弹性电子隧穿激发局域等离子体发光是另一种太赫兹荧光产生方法。Kimura等^[83]在 2021 年报道了太赫兹场驱动扫描隧道发光光谱研究,他们将最大电场强度为 188 V/cm 的太赫兹脉冲引导到低温扫描隧道显微镜的金针尖和银衬底隧穿节上,另一端使用透镜收集由太赫兹瞬变诱导的光子并将其引导至光谱仪中测量来自电子集体振荡(也就是等离子体激元的辐射衰变)的可见光子发射,如图 14 所示。研究发现:当遮挡太赫兹波时,光谱无明显峰;当引入太赫兹波时,光谱中出现一个从 1.3 eV 到 2.3 eV 的宽峰。这表明该荧光是由太赫兹脉冲产生的。该方法的原理如下:在金属-氧化层-金属结构中,当太赫兹波聚焦到针尖上时,就会驱动电子产生隧穿电流,隧穿电子与尖端、样品表面之间的电子振荡相互作用,隧穿结中局部等离子体激元的能量被位于靠近扫描隧道显微镜尖端的分子吸收,而尖端的接近平移不变性的损失,促使部分隧穿电子转换成光子,从而导致光致发光。

3.5 太赫兹波诱导高次谐波产生

在强激光与物质相互作用过程中,当电场强度达到甚至超过物质内部原子或分子间的库仑势时,就会引发一系列的极端非线性物理现象,如背向散射^[84]、阈上电离^[85]、高次谐波产生^[86]等。高次谐波由于时域脉冲短、波长可调谐、物理内涵丰富等优势而备受关注。

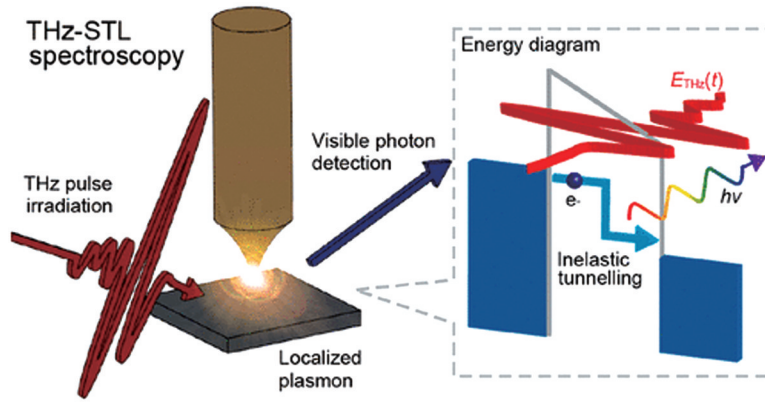


图 14 太赫兹扫描隧道发光测量原理图^[83](图中给出了针尖和样品,插图表示发光原理:由太赫兹场驱动的非弹性隧穿电子诱导局域等离子体发光)

Fig. 14 Schematic of THz-STL measurement^[83] (the figure shows the tip and sample and the inset shows the luminescence principle: luminescence from a localized plasmon is induced by THz-field-driven inelastically tunneled electrons)

一般情况下,提高入射激光的聚焦强度可以有效增强高次谐波的发射强度,但这样往往会超过很多固体样品的损伤阈值,从而对样品造成不可逆转的损伤。太赫兹波的光子能量较低,并且飞秒量级的太赫兹场强不受直流介电击穿效应的限制,因此其可以聚焦到样

品上得到远超过物质静态介电强度的光场强度而不损伤样品,从而引发一系列高阶非线性光学效应。2014年, Schubert 等^[87]利用中心频率为 30 THz、场强高达 72 MV/cm 的太赫兹波辐射半导体 GaSe,观察到了最高至 22 阶的谐波产生,如图 15 所示。理论计算结果表

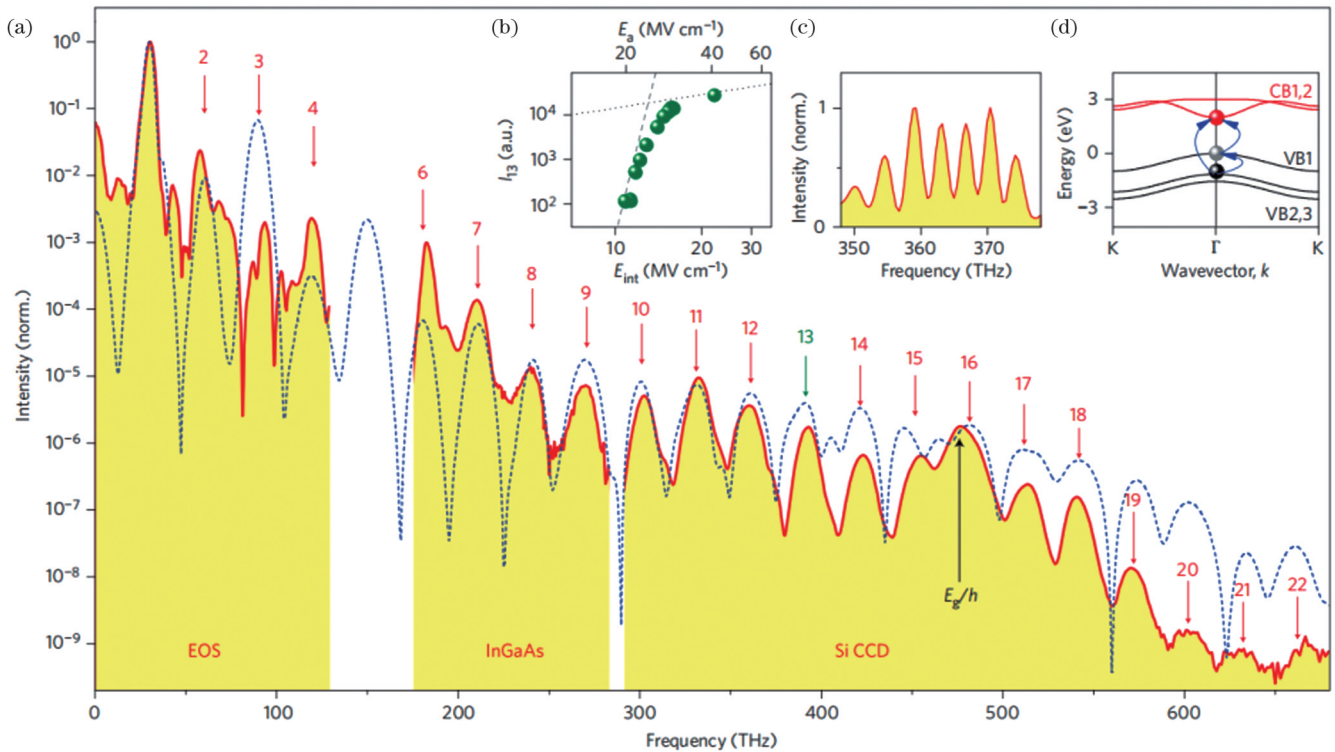


图 15 块体 GaSe 中载波包络相位稳定的太赫兹波高次谐波产生^[87]。(a)由相位锁定的太赫兹脉冲驱动 GaSe 单晶发射的高次谐波强度谱图(实线和阴影区域);(b)第 13 阶谐波强度 I_{13} 与入射太赫兹波幅值 E_0 (顶标尺)以及晶体表面反射的太赫兹场强 E_{int} (底标尺);(c)倍频的 6 阶谐波和 12 阶谐波之间的频谱干扰证实了高次谐波辐射的稳定性;(d)GaSe 在 G 点和 K 点之间的电子能带色散

Fig. 15 Carrier-envelope phase-stable terahertz high-harmonic generation in bulk GaSe^[87]. (a) High-harmonic intensity spectrum (solid line and shaded area) emitted from a GaSe single crystal driven by the phase-locked terahertz pulse; (b) dependence of the intensity I_{13} of the 13th harmonic on the incident terahertz amplitude E_0 (top scale) and the terahertz field strength E_{int} (bottom scale) obtained from E_0 by accounting for reflection at the crystal surface; (c) the spectral interference between the frequency-doubled sixth harmonic and 12th harmonic confirms the stability of the high-harmonic radiation; (d) electronic band dispersion of GaSe between the G- and K-points

明,高次谐波的产生起源于动态布洛赫振荡与相干带间激发的结合。激发的电子可以在不到太赫兹波半个周期内被加速到布里渊区边界,对应的布洛赫周期只有数飞秒,这种动态变化会导致高频辐射,并且与入射太赫兹波的载波包络相位有关。2015年, Schubert 所在团队^[88]在时域光谱中直接观测到了高次谐波产生,这种高次谐波是由一连串亚周期组成的,并且在时间上与驱动的太赫兹波的一个波峰重合,这表明该过程

涉及多个能带间电子跃迁的非微扰性量子干涉。

Bowlan 等^[89]利用时间分辨太赫兹光谱技术,在多层外延石墨烯中也观测到了高次谐波产生。太赫兹电场作用于带内和带间电荷流,以相干驱动载流子的运动,从而产生高次谐波。2018年, Hafez 等^[90]发现:在室温条件下,只用数十 kV/cm 场强的太赫兹脉冲辐照石墨烯即可产生高达 7 阶的太赫兹谐波,并且具有较高的转换效率,如图 16 所示。这种太赫兹谐波的产生

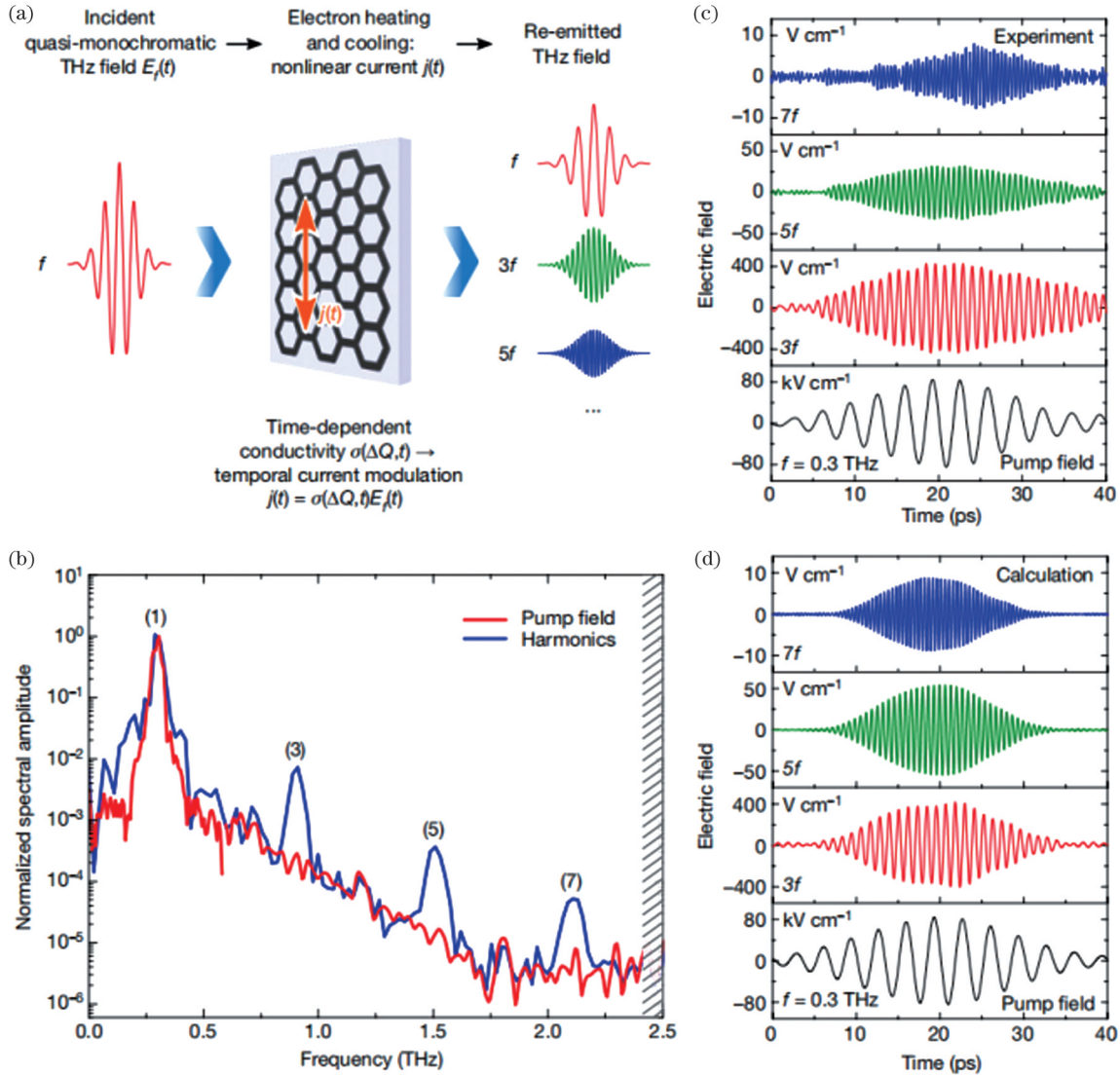


图 16 太赫兹高次谐波产生原理及主要结果^[90]。(a)实验示意图;(b)太赫兹诱导的高次谐波(红线为频率 $f=0.3$ THz、峰值强度 $E_i=85$ kV/cm 的入射太赫兹幅度光谱;蓝线为同一太赫兹波通过石墨烯的频谱,清晰可见产生的 3 阶、5 阶和 7 阶谐波;阴影区域表示探测器截止点);(c)泵浦光(黑线)以及(b)图情况下产生的第 3、第 5、第 7 阶太赫兹谐波;(d)热力学模型计算,对应于 (b)和(c)图中的测量,将频率 $f=0.3$ THz 的基频光(黑线)和石墨烯在 300 K 完全热平衡时的基本参数作为输入参数

Fig. 16 Schematic and main results of the THz high-harmonic generation^[90]. (a) Schematic of the experiment; (b) terahertz induced high harmonics (red line, amplitude spectrum of the incident pump THz wave at the fundamental frequency $f=0.3$ THz with peak field strength $E_i=85$ kV/cm, determined in the reference measurement. Blue line, the spectrum of the same THz wave transmitted through graphene on a substrate, with clearly visible generated harmonics of third, fifth and seventh order. The shaded area represents the detector cut-off); (c) pump wave (black line) and generated third, fifth and seventh THz harmonics for the case in Fig. (b); (d) thermodynamic model calculation, corresponding to the measurements in Figs. (b) and (c), using the experimental fundamental pump wave at frequency $f=0.3$ THz (black line) and the basic parameters of graphene in full thermal equilibrium at 300 K as input parameters

原理是石墨烯中狄拉克电子对驱动太赫兹场的准瞬态集体热响应的极端非线性行为,并且这一原理理论上可以推广到其他具有狄拉克或外尔费米子的拓扑材料中。Schmid 等^[91]在拓扑绝缘体 Bi_2Te_3 中观测到了高效的太赫兹波驱动的高次谐波产生,如图 17 所示。由于体内窄带隙的存在,不同频率的太赫兹波驱动可以很

好地区分来自体内和拓扑表面态的高次谐波生成,其中由自旋动量锁定和准相对论色散而产生的长散射时间使得高次谐波生成异常有效。另外,通过改变驱动太赫兹波电场的载流子包络相位,所有观察到的阶次的频率都可以连续地移动到任意非整数倍基频的频率上,这与量子理论一致。

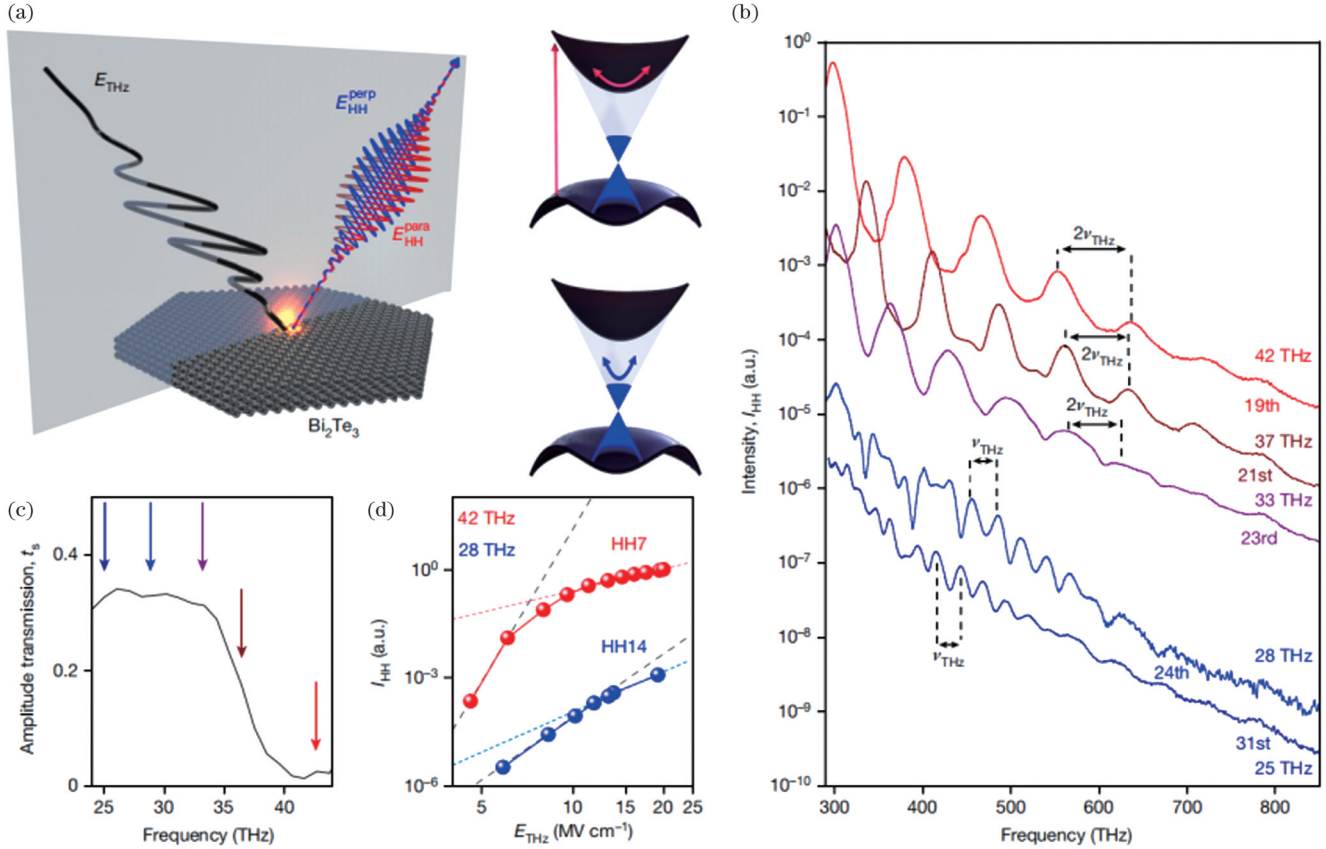


图 17 拓扑绝缘体的高次谐波发射^[91]。(a)实验原理图,其中右图分别表示体(上)和表面(下)产生的高次谐波,浅灰色表示狄拉克色散,深灰色表示抛物线型能带;(b)25 THz 和 42 THz 之间的 5 个驱动太赫兹波频率的高次谐波频谱图;(c)通过太赫兹时域光谱得到 6.5 μm 厚 Bi_2Te_3 晶体的振幅透射率 t_s ,其中 37 THz 处的边缘对应于体带隙,彩色箭头标记了(b)图中太赫兹波形的频率;(d)太赫兹电场依赖的 7 阶和 14 阶谐波强度

Fig. 17 High-harmonic emission from a topological insulator^[91]. (a) Experimental scheme, where the right sketches represent the high-order harmonic generation from the bulk (top) and the surface (bottom), respectively, and the light gray represents Dirac-like dispersion of the TSS and the dark gray represents parabolic bulk bands; (b) high-order harmonic spectra for five driving frequencies between 25 THz and 42 THz; (c) amplitude transmission, t_s , of a 6.5 μm thick Bi_2Te_3 crystal, obtained by THz time-domain spectroscopy, where the edge at about 37 THz corresponds to the bulk bandgap, and the coloured arrows mark the frequencies of the THz waveforms in Fig. (b); (d) intensity of 7th and 14th order harmonic as a function of THz electric field

3.6 太赫兹克尔效应

当太赫兹波入射到克尔介质时,其强电场分量会引发介质的三阶非线性效应,此时平行于和垂直于电场分量的折射率变得不同,发生双折射效应,即发生太赫兹克尔效应。该效应区别于普克尔效应(即线性电光效应),普克尔效应折射率的变化与外加场强成正比,如常用的 ZnTe 晶体电光采样原理^[92],而克尔效应折射率的变化与外加场强的平方成正比^[93-95]。2009 年, Hoffmann 等^[93]利用强度超过 100 kV/cm 的太赫兹脉冲激发苯、 CCl_4 等溶液首次证明了太赫兹克尔效应,即其引起的折射率变化与太赫兹波电场的平方成正

比。时间分辨的太赫兹克尔信号包含一个快弛豫分量和一个慢弛豫分量,分别对应于电子响应和核响应。

3.7 强场太赫兹波在生物医药领域中的应用

由于对分子结构和化学浓度的高度敏感性,太赫兹技术在生物医学领域也显示出了独特优势——用于诊断太赫兹波对不同生物组织的作用效果以及检测生物组织的性能,从而促进人们对生物系统的理解。生物系统的运作需要在液体环境中进行,然而,水的氢键网络对太赫兹波有强吸收,1 mm 厚的水膜能将频率为 1 THz 的太赫兹波的辐射强度衰减为原始值的 $1/10$ ^[96]。因此,为了使太赫兹辐射穿透液体环境并到

达生物系统, 高峰值功率是必要的。另外, 太赫兹辐射源应具有较低的平均功率, 以尽量减小可能对生物系统产生重大影响的热效应^[97-100]。目前, 强场太赫兹技术已被应用到生物医药领域, 越来越多的证据显示高强度太赫兹辐照确实可以对生物组织中的特定结构造成影响, 而其他组织则不受或受较弱影响, 如太赫兹辐照可以分解肌动蛋白微丝增强渗透性^[101], 影响哺乳动物干细胞的细胞分化^[102-103], 调控 DNA^[104], 对癌细胞进行处理^[97, 105]等。但是, 目前太赫兹辐照效应的广泛应用也存在巨大挑战。水的强吸收目前还是生物探测的巨大障碍, 水的太赫兹信号比生物分子的信号强, 从而影响了检测的准确性。发展更高、更强的太赫兹源是解决方案之一。另外, 设计新型的探测方式, 如将纳米技术和太赫兹技术相结合^[99]等, 也可以提高探测效率。此外, 数据分析和解释也是一大障碍, 现有的理论模拟模型还有待完善。

4 结束语

本文首先介绍了几种常见的强场太赫兹源产生方式, 随后针对强场太赫兹技术在物性调控方面的应用, 简单介绍了强场太赫兹波在物质中引起的一些物理现象, 包括强场驱动热载流子运动、相干电子或声子调控、强场自旋电子学、太赫兹荧光发射、太赫兹克尔效应等。

随着科技的进步, 强太赫兹源正变得越来越容易获得, 太赫兹探测技术也在不断进步, 现在已经可以使用不同的实验技术来探测各种非线性太赫兹现象。与此同时, 太赫兹的应用范围也在不断扩大, 许多极端环境(如极低温、强场、强磁、高压等)下的太赫兹光谱测量也应运而生。然而, 这也带来了一系列问题, 如, 稳定高效率的强场太赫兹源尚不能获得, 强场太赫兹波与物质相互作用的深层物理机制尚不明晰。另外, 在基础物理上有重大突破的新型太赫兹理论还未出现, 理论方面仍然存在着所谓的“太赫兹间隙”, 统一电磁理论和量子理论来解释新的太赫兹物理问题还亟待解决。这些问题的答案不仅对于基础科学的进步很重要, 而且与应用技术的发展密不可分。相信在不久的将来, 太赫兹技术势必会有重大突破, 太赫兹器件也会像可见光和近红外光器件那样被广泛运用到生活中的每个角落。

参 考 文 献

- [1] Isgandarov E, Ropagnol X, Singh M, et al. Intense terahertz generation from photoconductive antennas[J]. *Frontiers of Optoelectronics*, 2021, 14(1): 64-93.
- [2] Budiarto E, Margolies J, Jeong S, et al. High-intensity terahertz pulses at 1-kHz repetition rate[J]. *IEEE Journal of Quantum Electronics*, 1996, 32(10): 1839-1846.
- [3] Ropagnol X, Kovács Z, Gilicze B, et al. Intense sub-terahertz radiation from wide-bandgap semiconductor based large-aperture photoconductive antennas pumped by UV lasers[J]. *New Journal of Physics*, 2019, 21(11): 113042.
- [4] Ropagnol X, Morandotti R, Ozaki T, et al. Toward high-power terahertz emitters using large aperture ZnSe photoconductive antennas[J]. *IEEE Photonics Journal*, 2011, 3(2): 174-186.
- [5] Ropagnol X, Bouvier M, Reid M, et al. Improvement in thermal barriers to intense terahertz generation from photoconductive antennas[J]. *Journal of Applied Physics*, 2014, 116(4): 043107.
- [6] Holzman J F, Elezzabi A Y. Two-photon photoconductive terahertz generation in ZnSe[J]. *Applied Physics Letters*, 2003, 83(14): 2967-2969.
- [7] Kononenko V V, Komlenok M S, Chizhov P A, et al. Efficiency of photoconductive terahertz generation in nitrogen-doped diamonds[J]. *Photonics*, 2021, 9(1): 18.
- [8] Auston D H, Cheung K P, Smith P R. Picosecond photoconducting hertzian dipoles[J]. *Applied Physics Letters*, 1984, 45(3): 284-286.
- [9] Yang K H, Richards P L, Shen Y R. Generation of far-infrared radiation by picosecond light pulses in LiNbO₃[J]. *Applied Physics Letters*, 1971, 19(9): 320-323.
- [10] Morris J R, Shen Y R. Far-infrared generation by picosecond pulses in electro-optical materials[J]. *Optics Communications*, 1971, 3(2): 81-84.
- [11] Hirori H, Tanaka K. Dynamical nonlinear interactions of solids with strong terahertz pulses[J]. *Journal of the Physical Society of Japan*, 2016, 85(8): 082001.
- [12] Guiramand L, Nkeck J E, Ropagnol X, et al. Near-optimal intense and powerful terahertz source by optical rectification in lithium niobate crystal[J]. *Photonics Research*, 2022, 10(2): 340-346.
- [13] Wu X J, Kong D Y, Hao S B, et al. Generation of 13.9-mJ terahertz radiation from lithium niobate materials[J]. *Advanced Materials*, 2023, 35(23): 2208947.
- [14] Hauri C P, Ruchert C, Vicario C, et al. Strong-field single-cycle THz pulses generated in an organic crystal[J]. *Applied Physics Letters*, 2011, 99(16): 161116.
- [15] Lee J A, Kim W T, Jazbinsek M, et al. X-shaped alignment of chromophores: potential alternative for efficient organic terahertz generators[J]. *Advanced Optical Materials*, 2020, 8(9): 1901921.
- [16] Kim S J, Kang B J, Puc U, et al. Highly nonlinear optical organic crystals for efficient terahertz wave generation, detection, and applications[J]. *Advanced Optical Materials*, 2021, 9(23): 2101019.
- [17] Balos V, de Cantoblanco C U, Wolf M, et al. Optical rectification and electro-optic sampling in quartz[J]. *Optics Express*, 2023, 31(8): 13317-13327.
- [18] Wei Y X, Le J M, Huang L, et al. Efficient generation of intense broadband terahertz pulses from quartz[J]. *Applied Physics Letters*, 2023, 122(8): 081105.
- [19] Fülöp J A, Tzortzakakis S, Kampfrath T. Laser-driven strong-field terahertz sources[J]. *Advanced Optical Materials*, 2020, 8(3): 1900681.
- [20] Hebling J, Almasi G, Kozma I Z, et al. Velocity matching by pulse front tilting for large area THz-pulse generation[J]. *Optics Express*, 2002, 10(21): 1161-1166.
- [21] Zhang B L, Ma Z Z, Ma J L, et al. 1.4-mJ high energy terahertz radiation from lithium niobates[J]. *Laser & Photonics Reviews*, 2021, 15(3): 2000295.
- [22] Jazbinsek M, Puc U, Abina A, et al. Organic crystals for THz photonics[J]. *Applied Sciences*, 2019, 9(5): 882.
- [23] Zhang X C, Ma X F, Jin Y, et al. Terahertz optical rectification from a nonlinear organic crystal[J]. *Applied Physics Letters*, 1992, 61(26): 3080-3082.
- [24] Vicario C, Jazbinsek M, Ovchinnikov A V, et al. High efficiency THz generation in DSTMS, DAST and OH1 pumped by Cr: forsterite laser[J]. *Optics Express*, 2015, 23(4): 4573-4580.
- [25] Vicario C, Ovchinnikov A V, Ashitkov S I, et al. Generation of 0.9-mJ THz pulses in DSTMS pumped by a Cr: Mg₂SiO₄ laser[J].

- Optics Letters, 2014, 39(23): 6632-6635.
- [26] Majkić A, Zgonik M, Petelin A, et al. Terahertz source at 9.4 THz based on a dual-wavelength infrared laser and quasi-phase matching in organic crystals OH1[J]. Applied Physics Letters, 2014, 105(14): 141115.
- [27] Rader C, Zaccardi Z B, Ho S H E, et al. A new standard in high-field terahertz generation: the organic nonlinear optical crystal PNPA[J]. ACS Photonics, 2022, 9(11): 3720-3726.
- [28] Cook D J, Hochstrasser R M. Intense terahertz pulses by four-wave rectification in air[J]. Optics Letters, 2000, 25(16): 1210-1212.
- [29] Oh T I, Yoo Y J, You Y S, et al. Generation of strong terahertz fields exceeding 8 MV/cm at 1 kHz and real-time beam profiling [J]. Applied Physics Letters, 2014, 105(4): 041103.
- [30] Koulouklidis A D, Gollner C, Shumakova V, et al. Observation of extremely efficient terahertz generation from mid-infrared two-color laser filaments[J]. Nature Communications, 2020, 11: 292.
- [31] Zhao T, Xie P Y, Wan H J, et al. Ultrathin MXene assemblies approach the intrinsic absorption limit in the 0.5–10 THz band[J]. Nature Photonics, 2023, 17(7): 622-628.
- [32] Sun W F, Wang X K, Zhang Y. Terahertz generation from laser-induced plasma[J]. Opto-Electronic Science, 2022, 1(8): 220003.
- [33] Liao G Q, Li Y T. Review of intense terahertz radiation from relativistic laser-produced plasmas[J]. IEEE Transactions on Plasma Science, 2019, 47(6): 3002-3008.
- [34] Yiwen E, Zhang L L, Tcypkin A, et al. Broadband THz sources from gases to liquids[J]. Ultrafast Science, 2021, 2021: 9892763.
- [35] Hamster H, Sullivan A, Gordon S, et al. Subpicosecond, electromagnetic pulses from intense laser-plasma interaction[J]. Physical Review Letters, 1993, 71(17): 2725-2728.
- [36] Sheng Z M, Mima K, Zhang J E, et al. Emission of electromagnetic pulses from laser wakefields through linear mode conversion[J]. Physical Review Letters, 2005, 94(9): 095003.
- [37] Liao G Q, Li Y T, Li C, et al. Bursts of terahertz radiation from large-scale plasmas irradiated by relativistic picosecond laser pulses [J]. Physical Review Letters, 2015, 114(25): 255001.
- [38] Liao G Q, Li Y T, Liu H, et al. Multimillijoule coherent terahertz bursts from picosecond laser-irradiated metal foils[J]. Proceedings of the National Academy of Sciences of the United States of America, 2019, 116(10): 3994-3999.
- [39] Ebbesen T W, Lezec H J, Ghaemi H F, et al. Extraordinary optical transmission through sub-wavelength hole arrays[J]. Nature, 1998, 391(6668): 667-669.
- [40] Seo M A, Park H R, Koo S M, et al. Terahertz field enhancement by a metallic nano slit operating beyond the skin-depth limit[J]. Nature Photonics, 2009, 3(3): 152-156.
- [41] Liu M K, Hwang H Y, Tao H, et al. Terahertz-field-induced insulator-to-metal transition in vanadium dioxide metamaterial[J]. Nature, 2012, 487(7407): 345-348.
- [42] Lee S, Baek S, Kim T T, et al. Metamaterials for enhanced optical responses and their application to active control of terahertz waves[J]. Advanced Materials, 2020, 32(35): 2000250.
- [43] Suresh Kumar N, Naidu K C B, Banerjee P, et al. A review on metamaterials for device applications[J]. Crystals, 2021, 11(5): 518.
- [44] Wang K L, Mittleman D M, van der Valk N C J, et al. Antenna effects in terahertz apertureless near-field optical microscopy[J]. Applied Physics Letters, 2004, 85(14): 2715-2717.
- [46] Kang J H, Kim D S, Park Q H. Local capacitor model for plasmonic electric field enhancement[J]. Physical Review Letters, 2009, 102(9): 093906.
- [47] Jelic V, Iwaszczuk K, Nguyen P H, et al. Ultrafast terahertz control of extreme tunnel currents through single atoms on a silicon surface[J]. Nature Physics, 2017, 13(6): 591-598.
- [48] Nguyen P, Rathje C, Hornig R J, et al. Coupling terahertz pulses to a scanning tunneling microscope[J]. Physics in Canada, 2015, 71(3): 157-160.
- [49] Peller D, Roelcke C, Kastner L Z, et al. Quantitative sampling of atomic-scale electromagnetic waveforms[J]. Nature Photonics, 2021, 15(2): 143-147.
- [50] Markelz A G, Asmar N G, Brar B, et al. Interband impact ionization by terahertz illumination of InAs heterostructures[J]. Applied Physics Letters, 1996, 69(26): 3975-3977.
- [51] Tarekegne A T, Hirori H, Tanaka K, et al. Impact ionization dynamics in silicon by MV/cm THz fields[J]. New Journal of Physics, 2017, 19(12): 123018.
- [52] Su F H, Blanchard F, Sharma G, et al. Terahertz pulse induced intervalley scattering in photoexcited GaAs[J]. Optics Express, 2009, 17(12): 9620-9629.
- [53] Xu S J, Huang D J, Liu Z, et al. Hydrostatic pressure effect of photocarrier dynamics in GaAs probed by time-resolved terahertz spectroscopy[J]. Optics Express, 2021, 29(9): 14058-14068.
- [54] Razzari L, Su F H, Sharma G, et al. Nonlinear ultrafast modulation of the optical absorption of intense few-cycle terahertz pulses in n-doped semiconductors[J]. Physical Review B, 2009, 79(19): 193204.
- [55] Zeiger H J, Vidal J, Cheng T K, et al. Theory for dispersive excitation of coherent phonons[J]. Physical Review B, 1992, 45(2): 768-778.
- [56] Johnson A, Moreno-Mencia D, Amuah E, et al. Ultrafast loss of lattice coherence in the light-induced structural phase transition of V_2O_3 [J]. Physical Review Letters, 2022, 129(25): 255701.
- [57] Zhang K, Su F H, Liu D Y, et al. Probing the electronic topological transitions of WTe_2 under pressure using ultrafast spectroscopy[EB/OL]. (2023-03-09)[2023-04-05]. <https://arxiv.org/abs/2303.04974>.
- [58] Maehrein S, Paarmann A, Wolf M, et al. Terahertz sum-frequency excitation of a Raman-active phonon[J]. Physical Review Letters, 2017, 119(12): 127402.
- [59] Mankowsky R, Först M, Cavalleri A. Non-equilibrium control of complex solids by nonlinear phononics[J]. Reports on Progress in Physics, 2016, 79(6): 064503.
- [60] Reinhoffer C, Pilch P, Reinold A, et al. High-order nonlinear terahertz probing of the two-band superconductor MgB_2 : third- and fifth-order harmonic generation[J]. Physical Review B, 2022, 106(21): 214514.
- [61] Sie E J, Nyby C M, Pemmaraju C D, et al. An ultrafast symmetry switch in a Weyl semimetal[J]. Nature, 2019, 565(7737): 61-66.
- [62] Vaswani C, Wang L L, Mudiyansele D, et al. Light-driven Raman coherence as a nonthermal route to ultrafast topology switching in a Dirac semimetal[J]. Physical Review X, 2020, 10(2): 021013.
- [63] Li X, Qiu T, Zhang J H, et al. Terahertz field - induced ferroelectricity in quantum paraelectric $SrTiO_3$ [J]. Science, 2018, 364(6445): 1079-1082.
- [64] Guo J X, Chen W W, Chen H S, et al. Recent progress in optical control of ferroelectric polarization[J]. Advanced Optical Materials, 2021, 9(23): 2002146.
- [65] Zhuang S H, Hu J M. Role of polarization-photon coupling in ultrafast terahertz excitation of ferroelectrics[J]. Physical Review B, 2022, 106(14): L140302.
- [66] Cheng B, Kramer P L, Shen Z X, et al. Terahertz-driven local dipolar correlation in a quantum paraelectric[J]. Physical Review Letters, 2023, 130(12): 126902.
- [67] Kampfrath T, Sell A, Klatt G, et al. Coherent terahertz control of antiferromagnetic spin waves[J]. Nature Photonics, 2011, 5(1): 31-34.
- [68] Barman A, Gubbiotti G, Ladak S, et al. The 2021 magnonics roadmap[J]. Journal of Physics: Condensed Matter, 2021, 33(41): 0413001.
- [69] Baltz V, Manchon A, Tsoi M, et al. Antiferromagnetic spintronics [J]. Reviews of Modern Physics, 2018, 90(1): 015005.
- [70] Gomonay E V, Loktev V M. Spintronics of antiferromagnetic

- systems (review article)[J]. *Low Temperature Physics*, 2014, 40(1): 17-35.
- [71] Salén P, Basini M, Bonetti S, et al. Matter manipulation with extreme terahertz light: progress in the enabling THz technology[J]. *Physics Reports*, 2019, 836/837: 1-74.
- [72] Jin Z M, Mics Z, Ma G H, et al. Single-pulse terahertz coherent control of spin resonance in the canted antiferromagnet YFeO_3 , mediated by dielectric anisotropy[J]. *Physical Review B*, 2013, 87(9): 094422.
- [73] Mashkovich E A, Grishunin K A, Dubrovin R M, et al. Terahertz light - driven coupling of antiferromagnetic spins to lattice[J]. *Science*, 2021, 374(6575): 1608-1611.
- [74] Baierl S, Mentink J H, Hohenleutner M, et al. Terahertz-driven nonlinear spin response of antiferromagnetic nickel oxide[J]. *Physical Review Letters*, 2016, 117(19): 197201.
- [75] Vicario C, Ruchert C, Ardana-Lamas F, et al. Off-resonant magnetization dynamics phase-locked to an intense phase-stable terahertz transient[J]. *Nature Photonics*, 2013, 7(9): 720-723.
- [76] Bonetti S, Hoffmann M C, Sher M J, et al. THz-driven ultrafast spin-lattice scattering in amorphous metallic ferromagnets[J]. *Physical Review Letters*, 2016, 117(8): 087205.
- [77] Schlauderer S, Lange C, Baierl S, et al. Temporal and spectral fingerprints of ultrafast all-coherent spin switching[J]. *Nature*, 2019, 569(7756): 383-387.
- [78] Baierl S, Hohenleutner M, Kampfrath T, et al. Nonlinear spin control by terahertz-driven anisotropy fields[J]. *Nature Photonics*, 2016, 10(11): 715-718.
- [79] Seifert T, Jaiswal S, Martens U, et al. Efficient metallic spintronic emitters of ultrabroadband terahertz radiation[J]. *Nature Photonics*, 2016, 10(7): 483-488.
- [80] Liao G Q, Li Y T, Liu H, et al. Multimillijoule coherent terahertz bursts from picosecond laser-irradiated metal foils[J]. *Proceedings of the National Academy of Sciences of the United States of America*, 2019, 116(10): 3994-3999.
- [81] Shi J J, Yoo D, Vidal-Codina F, et al. A room-temperature polarization-sensitive CMOS terahertz camera based on quantum-dot-enhanced terahertz-to-visible photon upconversion[J]. *Nature Nanotechnology*, 2022, 17(12): 1288-1293.
- [82] Pein B C, Chang W D, Hwang H Y, et al. Terahertz-driven luminescence and colossal stark effect in CdSe-CdS colloidal quantum dots[J]. *Nano Letters*, 2017, 17(9): 5375-5380.
- [83] Kimura K, Morinaga Y, Imada H, et al. Terahertz-field-driven scanning tunneling luminescence spectroscopy[J]. *ACS Photonics*, 2021, 8(4): 982-987.
- [84] Blaga C I, Catoire F, Colosimo P, et al. Strong-field photoionization revisited[J]. *Nature Physics*, 2009, 5(5): 335-338.
- [85] Corkum P B, Burnett N H, Brunel F. Above-threshold ionization in the long-wavelength limit[J]. *Physical Review Letters*, 1989, 62(11): 1259-1262.
- [86] Krause J L, Schafer K J, Kulander K C. High-order harmonic generation from atoms and ions in the high intensity regime[J]. *Physical Review Letters*, 1992, 68(24): 3535-3538.
- [87] Schubert O, Hohenleutner M, Langer F, et al. Sub-cycle control of terahertz high-harmonic generation by dynamical Bloch oscillations[J]. *Nature Photonics*, 2014, 8(2): 119-123.
- [88] Hohenleutner M, Langer F, Schubert O, et al. Real-time observation of interfering crystal electrons in high-harmonic generation[J]. *Nature*, 2015, 523(7562): 572-575.
- [89] Bowlan P, Martinez-Moreno E, Reimann K, et al. Ultrafast terahertz response of multilayer graphene in the nonperturbative regime[J]. *Physical Review B*, 2014, 89(4): 041408.
- [90] Hafez H A, Kovalev S, Deinert J C, et al. Extremely efficient terahertz high-harmonic generation in graphene by hot Dirac fermions[J]. *Nature*, 2018, 561(7724): 507-511.
- [91] Schmid C P, Weigl L, Grössing P, et al. Tunable non-integer high-harmonic generation in a topological insulator[J]. *Nature*, 2021, 593(7859): 385-390.
- [92] Planken P C M, Nienhuys H K, Bakker H J, et al. Measurement and calculation of the orientation dependence of terahertz pulse detection in ZnTe[J]. *Journal of the Optical Society of America B*, 2001, 18(3): 313-317.
- [93] Hoffmann M C, Brandt N C, Hwang H Y, et al. Terahertz Kerr effect[J]. *Applied Physics Letters*, 2009, 95(23): 231105.
- [94] Kampfrath T, Campen R K, Wolf M, et al. The nature of the dielectric response of methanol revealed by the terahertz Kerr effect [J]. *The Journal of Physical Chemistry Letters*, 2018, 9(6): 1279-1283.
- [95] Zhao H, Tan Y, Zhang R, et al. Anion - water hydrogen bond vibration revealed by the terahertz Kerr effect[J]. *Optics Letters*, 2021, 46(2): 230-233.
- [96] Xu J, Plaxco K W, Allen S J. Absorption spectra of liquid water and aqueous buffers between 0.3 and 3.72 THz[J]. *The Journal of Chemical Physics*, 2006, 124(3): 036101.
- [97] Hough C M, Purschke D N, Huang C X, et al. Intense terahertz pulses inhibit Ras signaling and other cancer-associated signaling pathways in human skin tissue models[J]. *Journal of Physics: Photonics*, 2021, 3(3): 034004.
- [98] Weightman P. Prospects for the study of biological systems with high power sources of terahertz radiation[J]. *Physical Biology*, 2012, 9(5): 053001.
- [99] Zhou R Y, Wang C, Xu W D, et al. Biological applications of terahertz technology based on nanomaterials and nanostructures[J]. *Nanoscale*, 2019, 11(8): 3445-3457.
- [100] Liu W, Liu Y, Huang J Q, et al. Application of terahertz spectroscopy in biomolecule detection[J]. *Frontiers in Laboratory Medicine*, 2018, 2(4): 127-133.
- [101] Yamazaki S, Harata M, Ueno Y, et al. Propagation of THz irradiation energy through aqueous layers: demolition of actin filaments in living cells[J]. *Scientific Reports*, 2020, 10: 9008.
- [102] Bock J, Fukuyo Y, Kang S, et al. Mammalian stem cells reprogramming in response to terahertz radiation[J]. *PLoS One*, 2010, 5(12): e15806.
- [103] Kim K T, Park J, Jo S J, et al. High-power femtosecond-terahertz pulse induces a wound response in mouse skin[J]. *Scientific Reports*, 2013, 3: 2296.
- [104] Titova L V, Ayesheshim A K, Golubov A, et al. Intense THz pulses cause H2AX phosphorylation and activate DNA damage response in human skin tissue[J]. *Biomedical Optics Express*, 2013, 4(4): 559-568.
- [105] Cheon H, Paik J H, Choi M, et al. Detection and manipulation of methylation in blood cancer DNA using terahertz radiation[J]. *Scientific Reports*, 2019, 9: 6413.

Intense Terahertz Generation and Its Applications in Nonlinear Research

Wang Tianwu^{1,2,3,4,5*}, Zhang Kai^{1,2}, Wei Wenjin^{1,2}, Li Hongbo^{1,2,3,4,5}, Zhou Zhipeng^{1,2},
Cao Ling^{1,2}, Li Hong^{1,2}, Fang Guangyou^{1,2,3,4,5}, Wu Yirong^{1,2,3,4,5}

¹*GBA Branch of Aerospace Information Research Institute, Chinese Academy of Sciences, Guangzhou 510700, Guangdong, China;*

²*Guangdong Provincial Key Laboratory of Terahertz Quantum Electromagnetics, Guangzhou 510700, Guangdong, China;*

³*Key Laboratory of Electromagnetic Radiation and Sensing Technology, Chinese Academy of Sciences, Beijing 100190, China;*

⁴*Aerospace Information Research Institute, Chinese Academy of Sciences, Beijing 100101, China;*

⁵*School of Electronic, Electrical and Communication Engineering, University of Chinese Academy of Sciences, Beijing 100049, China*

Abstract

Significance As an important research method, spectroscopy exhibits versatile and unique advantages, such as contactless measurement, high sensitivity, and convenience, and thus is widely used in material science and engineering. With increasing progress of science and technology, the branches of spectroscopy have gradually broadened, and a variety of complex functional spectral analysis technologies have emerged. Among those, ultrafast spectroscopy is an important subject that has developed rapidly in recent years. It introduces the time degree of freedom on the basis of traditional steady-state spectroscopy, subdivides the interaction between light and matter at the picosecond time scale, and studies the time-resolved dynamics of such quasi-particles as hot carriers, phonons, polarons, and excitons in matter. At present, the wavelengths of light used in ultrafast spectroscopy have covered most of the bands in the electromagnetic spectrum, and its scope of application has also extended deeply into condensed matter physics, material science, biomedicine, military, and national defense. Terahertz spectroscopy is an important branch of ultrafast spectroscopy used in technology that developed in the 1980s that has important scientific research and application prospects. Generally, as commonly defined, terahertz (THz) waves refer to electromagnetic waves with frequencies in the range 0.1–10 THz (wavelength 3 mm–30 μm), also known as submillimeter waves or terahertz radiation. Electromagnetic waves in this band exhibit many useful properties, such as low photon energy, high penetration, a close match with molecular vibration and rotational energy levels, and no harmful radiation. Thus, THz radiation has found a wide range of use nowadays. Terahertz technology therefore has become a major emerging field of science and technology in the 21st century. It is rated as one of the top 10 technologies that will change the world of the future by the United States, and has been highly evaluated by governments around the world.

With the continued progress of terahertz technology, the terahertz emission efficiency of materials has continually increased, and the corresponding electromagnetic field intensity has also gradually increased. The electric field component of intense terahertz waves can easily reach MV/cm magnitudes, and its corresponding magnetic field component can reach Tesla magnitudes. When a sample is irradiated with such intense terahertz waves, the strong electromagnetic field can apparently regulate the internal physical properties of matter, such as its spin/electron/lattice structure, dielectric property, and susceptibility, resulting in a series of nonlinear responses, such as collision ionization, valley scattering, and the terahertz Kerr effect. Research on these nonlinear effects can clarify these phenomena, promoting the development of ultrafast optoelectronic devices.

Progress Intense terahertz waves exhibit high peak power and correspondingly large amplitudes of the electric and magnetic field components, whereby they can induce numerous novel anomalous phenomena. In this paper, we first introduce some frequency used intense terahertz emission sources, including photoconductive antennas, optical rectification crystals, solid and gas plasma emissions, metamaterials, and tip enhancement. Some typical applications of intense terahertz technology in material science are also introduced, including collision ionization, intervalley scattering, coherent modulation, spin regulation, terahertz fluorescence, terahertz high order harmonic generation, terahertz Kerr effect, and biomedical uses.

Conclusions and Prospects With advances in technology, intense terahertz sources have become increasingly readily available, and terahertz detection techniques are also continuously growing. Currently, a wide range of experimental methods are being applied to detect a variety of nonlinear terahertz phenomena. In addition, the range of application of intense terahertz spectroscopy is also expanding, whereby measurements of physical properties of substances under extreme environmental conditions such as extremely low temperatures, strong electric and magnetic fields, and high pressure can now be performed. However, a series of problems also exists, such as the need for stable and efficient intense terahertz sources and a deep understanding of the physical mechanism underlying the interaction between intense terahertz waves and matter. In addition, a new terahertz theory to account for major breakthroughs in basic physics has not yet appeared, and there remains a so-called “terahertz gap” in theory. A combination of electromagnetic theory and quantum theory to solve new terahertz physics problems is needed. The answers to these questions are important not only for the progress of basic science, but also for the development of applied technology. We believe that in the near future, terahertz technology is bound to see major breakthroughs, whereupon terahertz devices will be as widely used in every corner of life as visible and near-infrared devices.

Key words ultrafast optics; intense terahertz source; intense terahertz modulation; applications of terahertz radiation